Ocean Engineering 292 (2024) 116452

Contents lists available at ScienceDirect

Ocean Engineering

journal homepage: www.elsevier.com/locate/oceaneng

Research paper

Estimation of probability of capsizing with split-time method

Vadim Belenky [a,*], Kenneth M. Weems [a], Woei-Min Lin [b], Vladas Pipiras [c], Themistoklis P. Sapsis [d]

[a] David Taylor Model Basin, Naval Surface Warfare Center Carderock Division, USA
[b] Office of Naval Research, USA
[c] University of North Carolina Chapel Hill, USA
[d] Massachusetts Institute of Technology, USA

ARTICLE INFO

Handling Editor: Prof. A.I. Incecik

Keywords:
Probability of capsizing
Statistic of extremes

ABSTRACT

The paper summarizes almost three decades of research on the probability of ship capsizing in irregular waves. Reduced-order models (ROM) of roll with piecewise linear restoring are described. ROMs are capable of the presentation of the key feature of capsizing: transition to motions about upside-down stable equilibrium. The insight gained with these ROMs has paved the way towards a split-time method for engineering-level simulation tools. The modeling divides the capsizing problem into two parts: the upcrossing of an intermediate roll angle and the probability of capsizing after upcrossing. The split-time method enables a statistical characterization of capsizing event without observing one, using perturbation to generate synthetic data, containing information on the instantaneous likelihood of capsizing and enabling the application of extreme value theory.

1. Introduction

1.1. Capsizing as a random event

The capsizing of a ship is the worst possible outcome of a stability failure. As a result, the probability of capsizing in realistic (i.e., random) seas is a natural criterion for the stability of a ship. Capsizing is a random event in irregular waves, so the concept of probability is fully applicable as probability is a measure of the likelihood of a random event. The rationality of a stability criterion expressed in terms of probability was considered by Kobylinski (1975).

The probability of a random event occurring during a certain time interval (e.g. service life of a ship) is related to the duration of this interval. Sevastianov (1963) considered the relationship of probability and time, particularly for the assessment of ship stability. The recognition of the relationship between time and probability casts the assessment of ship stability as a general reliability problem (Sevastianov, 1982, 1994; Caldwell and Yang, 1986, Chapter 1 of Belenky and Sevastianov 2007). In the International Maritime Organization (IMO) Second Generation Intact Stability Criteria, see Section 3 of MSC.1/Circ. 1627 (IMO, 2020), this relation is modeled as a Poisson process and performed within the probabilistic framework of direct stability assessment. Its theoretical background is available in Section 2 of SDC 8/INF.2 (IMO, 2021). For a Poisson process, the probability of k events occurring within a time interval T is expressed as:

$$P(k) = \frac{(rT)^k}{k!} \exp(-rT) \tag{1}$$

where r is the rate of random events. The rate r is usually interpreted as the probability of an event per unit of time. The probability of no events (i.e., no capsizing) corresponds to $k = 0$.

Physically, capsizing is a transition from roll motions near one stable equilibrium to motions near another (upside-down) stable equilibrium, as illustrated in Fig. 1. While in real practice, the upside down equilibrium, most probably, will not occur due to machinery and cargo shifting, structural damage, downflooding, etc., it is still useful for a theoretical definition.

A dynamical system capable of describing this transition has to include at least two stabile equilibria (upright and upside-down) as well as an unstable equilibrium between these two (angle of vanishing stability). This dynamical system is characterized by a significant nonlinearity. While the irregular sea wave elevations can be assumed Gaussian, the nonlinearity of the dynamical system means that the roll response will not have a Gaussian distribution. Moreover, capsizing is likely to violate the stationarity of the roll response process. These complexities leave time-domain simulation as the only way to model the capsizing of

* Corresponding author.
E-mail address: vadim.belenky@navy.mil (V. Belenky).

https://doi.org/10.1016/j.oceaneng.2023.116452
Received 24 May 2023; Received in revised form 20 November 2023; Accepted 26 November 2023
Available online 22 December 2023
0029-8018/Published by Elsevier Ltd.

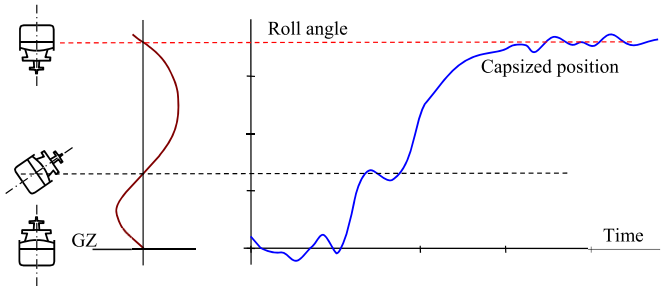

Fig. 1. Capsizing as a transition to motion near the inverted stable equilibrium.

a ship.

The capsizing of an undamaged ship in a normal operational condition is a rare event. As a result, the volume of sample, needed to estimate the probability of capsizing with direct time-domain numerical simulation, will be large, perhaps many thousand or even millions of hours. The computational cost of running an engineering-level numerical simulation to generate a sample of the required size is likely to be prohibitive. This situation is recognized as the problem of rarity in Section 3.5.1 of MSC.1/Circ. 1627 (IMO, 2020).

1.2. Probabilistic interpretation of weather criterion

A solution to the problem of rarity is a simplified model of capsizing. The weather criterion is one the most mature of such simplified models, see Section 2.3 of the IS Code (IMO, 2008). The probabilistic interpretation of the weather criterion seems to be a logical approach (e.g., Dudziak and Buczkowski, 1978), abridged version available in the Section 9.3.2 of (Belenky and Sevastianov, 2007). The result, however, is not consistent when compared with the probability, estimated from Monte-Carlo simulations, since it cannot be uniquely interpreted in terms of a choice of parameters values (Thanou, 2010; Peters and Belenky, 2023).

1.3. Distribution of large roll angles and its tail

Another approach is to approximate the distribution of the roll response in order to estimate the probability of exceedance of some large roll angle. This approach is reasonable as the influence of the unstable equilibrium on the distribution is limited to a relatively small interval close to this equilibrium (Belenky et al., 2019). As a result, the event of exceedance of an angle near the unstable equilibrium may have a probability that is not that different from the probability of capsizing. This feature is a result of the more general property that the shape of roll angle distribution is mostly defined by hydrostatics, i.e., by the geometry of the hull. The relationship between the hull geometry and roll distribution was noted some time ago, as reported in the Section 8.6.2 of Belenky and Sevastianov (2007).

Haddara and Zhang (1994) and Belenky (1994) approximated the distribution of roll angle with estimates of high-order moments, skewness and excess of kurtosis – using Gram-Charlier and Edgeworth series. The method presents the probability density function (PDF) in terms of its moments and can be derived with the Hermite polynomials e.g., Section 8.6.2 of (Belenky and Sevastianov, 2007). While the method seems to be working for small-to-moderate nonlinearity, attempts to apply it to a case with a larger nonlinearity like the Office of Naval Research (ONR) Topside Series Tumblehome hull (Bishop et al., 2005), lead to oscillations of a curve approximating the PDF of roll angles; due to these oscillations, the curve takes negative values, indicating a bad approximation (Fig. 10 in Belenky and Weems, 2008). The authors have also considered the Pearson family of distributions, developed originally for biostatistics applications (Pearson, 1916). Further attempts to use the moment estimates for approximating the PDF of roll was abandoned because 1) relatively large uncertainty of the third- and fourth-order moment estimates caused by their sensitivity to outliers, and 2) how well this approximations represent the tail of the distribution was not clear.

One of the simplest mathematical models of large-amplitude roll motion is a single ordinary differential equation where the hydrostatic and Froude-Krylov (incident wave) forces are separated. It is essentially a linear roll equation, where the nonlinearity is reintroduced in the form of a calm-water roll restoring arm (GZ) curve, e.g., chapter 3.6 of (Belenky and Sevastianov, 2007):

$$(I_x + A_{44})\ddot{\phi} + B_{44}\dot{\phi} + \rho g \nabla\, GZ(\phi) = \rho g \nabla\, GM\, \alpha(t) \tag{2}$$

where I_x is the transverse moment of inertia of the "dry" hull, A_{44} is the added moment of inertia, B_{44} is the linear roll damping coefficient, ρ is water density, g is the acceleration of gravity, ∇ is volumetric displacement, ϕ is the roll angle measured with respect to the calm water level (i.e., in an absolute sense), a dot above the symbol identifies the time derivative, α is the angle of wave slope, and a dot above a symbol indicates a time derivative. Many variants of the model (2) exist. Some of them include additional terms for nonlinear roll damping and diffraction. Sometimes the angle of wave slope is substituted with the effective angle of wave slope that accounts for the finite size of a ship compare to the waves. The GZ curve is usually represented with a polynomial. In the case when cubic a parabola is applied, equation (2) becomes the Duffing equation.

While not describing the full nonlinearity of ship motion, resulting from inseparability of hydrostatic and Froude-Krylov forces, these mathematical models are useful for their simplicity. The polynomial representation of the nonlinear restoring facilitates an asymptotic treatment of the moments (e.g., Nekrasov, 1994). A further simplification would be to assume that wave excitation has a very broad spectrum, i.e., is white noise. This assumption makes the response a Markov process; its distribution becomes a solution of the Fokker-Plank-Kolmogorov (FPK) equation. Moreover, a distribution of the time to reach a specified level can be found; this formulation is known as the First Passage Problem.

FPK has been intensively engaged for the description of large-amplitude roll motions in irregular waves: Haddara (1974), Francescutto (1998), Francescutto and Naito (2004), Su and Falzarano (2013) to name a few. The FPK approach has two problems. First, the spectrum of the actual wave excitation is not that wide (wave slope angle is not actually white noise). Second, the FPK equation is a differential equation in partial derivatives so its solution is not trivial. Both of these problems can be solved. For the first, a filter can be applied to white noise to model realistic wave excitation. For the second, path integration has been found to be an efficient way to solve the FPK equation, describing roll motion (Naess and Moe, 2000). In Kougioumtzoglou and Spanos (2014), path integration solved the First Passage Problem for roll motions modeled with Duffing equations and obtained a favorable comparison with direct Monte-Carlo simulations.

Maki (2017) found a shape of the distribution by solving the FPK equation and assuming wave slope angle to be white noise. The autocorrelation of the excitation does not affect hydrostatics, so the FPK that accounts for the nonlinearity related to hull geometry reveals the shape of the PDF. The PDF can then be scaled with a variance estimate from a relatively short Monte-Carlo simulation, also Maki et al. (2019, 2022).

Actually, finding the entire distribution may not be necessary, as the extreme response is described by the tail of the distribution. Fitting the tail is the main subject of Campbell et al. (2023) and the reader is referred to that paper for a review of the tail-fitting approach.

The mathematical background for distribution tail fitting lies in the extreme value theory (e.g., Coles, 2001). The principle is that the distribution of the largest values in a sample asymptotically follows a Generalized Extreme Value (GEV) distribution and does not depend on the underlying distribution (of roll motion, for the relevant application).

The first application of GEV to the capsizing probability problem has been attributed to McTaggart (2000) and McTaggart and de Kat (2000).

1.4. Application of Crossing Theory and First-Order Reliability Method

One way to relate the probability of exceedance with time is to apply the Crossing Theory (e.g. Sections 10 through 12 of Kramer and Leadbetter (1967), and its "engineering" adaptation in Section 9.1 of Belenky and Sevastianov, 2007). The upcrossing of a level is defined as a random event when a stochastic process has reached that level with a positive derivative, while the downcrossing uses the negative derivative. These crossings asymptotically follow Poisson process (1). To compute the rate of crossing, the joint distribution of roll angles and rates must be known. For example, upcrossing rate of roll angle for the level a is expressed as (Kramer and Leadbetter, 1967):

$$r = \int_0^\infty \dot{\phi}\, \mathrm{PDF}(\phi, \dot{\phi}) d\dot{\phi} \tag{3}$$

where ϕ is an instantaneous roll angle and a dot above the symbol identifies the time derivative. The roll angles ϕ and rates $\dot{\phi}$ are not correlated, but the absence of correlation means independence only for a Gaussian process. As roll is not Gaussian, the independence of roll angles and rates is an assumption. Belenky and Weems (2019) have demonstrated that this assumption may hold for beam seas, but may not be valid for stern quartering seas where the stability variation in waves may be significant.

If the assumption of independence is valid, a good approximation of the PDF of roll angle facilitates the calculation of upcrossing rate (3). The distribution of roll rate is usually assumed Gaussian as it is related to the nonlinearity of roll damping, which is relatively weak, compared to the nonlinearity of hydrostatic restoring. The validity of this assumption is discussed further in Section 2.11.

Bulian and Francescutto (2004, 2011, 2011a) have avoided the difficulties of the approximation of the PDF of nonlinear roll. Instead, they considered an upcrossing of a linearized roll motion for an equivalent level of stability failure. This level is computed from a simplified energy balance of a nonlinear dynamical system, employing the principles of the weather criterion. The nonlinearity of the problem is essentially concentrated in the equivalent level of failure. The problem becomes linear and its rarity is addressed with a closed-form solution. The method was used for the formulation the second-generation intact stability criteria, see Section 2.2.3 of MSC.1/Circ. 1627 (IMO 2020). A brief description of theoretical background is available in Sections 3.3 and 3.4 of SDC 8/INF.2 (IMO 2021).

The linearization is also at the center of the First-Order Reliability Method (FORM). The non-Gaussian process of interest is transformed to a standard normal process, leading to an approximation for the crossing rate (Jensen and Capul, 2006). Literature on the application of FORM to large-amplitude ship motions is quite comprehensive, e.g., Jensen (2017), Jensen et al. (2017), Choi and Jensen (2019).

1.5. Critical wave group approach

In the transition from the upright to upside-down stable equilibrium, a ship needs to overcome a significant barrier, which can be expressed approximately as the area under the positive part of the GZ curve. To do so requires external energy from the waves. Obviously, capsizing is most likely to occur upon the encounter of a small number of large and steep waves within the random wave system. Sea waves have a group structure, so large waves are encountered in groups. Waves in a wave group are hydrodynamically related (Quasi-Determinism), see (Boccotti, 2000, 2014), and the probability of encountering a wave group is a reflection of this hydrodynamic relation.

Themelis and Spyrou (2007) considered a seaway as a sequence of dangerous wave groups separated by time intervals with only benign waves. As the wave groups are short (3–4 waves usually), the evaluation of a nonlinear ship response to a wave group is not an expensive calculation. A series of these evaluations can identify a critical wave group that would result in a large roll angle or capsizing. The probability (or rate) of encountering a critical wave group then provides an estimate of the probability of capsizing. Studies of the critical wave groups were directed toward better probabilistic models of the wave group themselves and the initial conditions upon encounter those wave groups (Anastopoulos and Spyrou, 2019, 2023). The computational efficiency of the wave group method allows the application of unsteady Reynolds-averaged Navier-Stokes (URANS) simulations (Silva and Maki, 2021, Silva and Maki, 2024) or physical model test (Anastopoulos et al., 2016; Bassler et al., 2019) to evaluate extreme ships responses. A subset of the critical wave group method, the critical wave method, is included in the IMO Interim Guidelines for the Second Generation Intact Stability Criteria, see Section 3.5.5.4 of MSC.1/Circ. 1627 (IMO 2020).

The application of the critical wave group method will involve a set of nonlinear dynamical simulations of the response to the wave group. Since these responses will depend on the initial conditions for the simulation, it is necessary to characterize the ship's conditions upon encountering a wave group. Those conditions are random, as they are result of the action of benign waves — the wave groups are assumed to be rare, so the system "forgets" encountering the previous wave group (s). Treatment of initial conditions for the critical wave group method is available from Themelis and Spyrou (2008) as well as from Anastopoulos and Spyrou (2019). Silva and Maki (2021) consider handling initial conditions for a URANS response simulation. Bassler et al. (2019) describe a possible model release mechanism, specially designed to control initial conditions for wave group experiments in a model tank.

1.6. Wave episode approach

The wave episode approach also uses the idea that capsizing results from a sequence of particularly large waves in an irregular seaway. It differs from the wave group approach as the hydrodynamic relation between the waves in the wave episode is not part of the formulation. Alford and Troesch (2009) describe a Dynamic Load Generator, which is based on a Longuett-Higgins model of irregular waves with amplitudes from a spectrum and random phases. The method searches for combinations of the phases that lead to an expected roll response (Kim and Troesch, 2013, 2019). Edwards et al. (2021) proposed improvements to the method with an equivalent linear dynamical system that has the same zero-crossing period as the system of interest.

To reduce the computational cost of high-fidelity simulation of a large-amplitude response, Mohamad and Sapsis (2018) employed adaptive sampling, which is based on Bayesian approach. The results of initial calculations are approximated with Gaussian process regression, which fits a mean value function of a non-stationary Gaussian process with available data (Rasmussen and Williams, 2006). These results are taken as "prior knowledge". As the Gaussian process regression comes with an uncertainty quantification, the conditions for the next calculation can be chosen to minimize the uncertainty — this is "*a posteriori* knowledge." The problem of initial conditions is considered by Guth and Sapsis (2022) with a "stochastic prelude" approach to capture the transitional behavior.

Reed (2021) proposed the identification of extreme response events with a qualitatively correct, body-nonlinear reduced-order model of ship motions in wave. This reduced-order model computes hydrostatic and Froude-Krylov forces with a volume of the instantaneous submerged portion of the hull and is fast enough to resolve the extremes with reasonable computational costs (Weems and Wundrow, 2013; Weems et al., 2018; Weems and Belenky, 2023). The idea is somewhat similar to the Design Load Generator: to find sets of time, position and component waves phases leading to extreme responses. The difference is that this set is found through a massive Monte-Carlo simulation, identifying a number of wave events were an extreme responses were observed. The

same wave events are then simulated with higher fidelity code (potential flow or URANS) to estimate the extreme response with engineering accuracy. The method strongly depends on the consistency between the reduced-order and engineering fidelity models (Weems et al., 2022). One of the advantages is that additional effort is not required to address the problem of initial conditions, as they can be taken directly from the ROM simulation.

1.7. Extrapolation over wave height

Another approach to the estimation of capsizing probability was proposed by Tonguć and Söding (1986). The probability of capsizing can be estimated with numerical time domain simulations in very severe sea conditions, for which capsizing becomes readily observable (i.e., not rare). The probability of capsizing in more realistic and less severe sea states can be found through extrapolation over the significant wave height. The method is included in the IMO interim guidelines for the Second Generation Intact Stability Criteria, see Section 3.5.5.3 of MSC.1/Circ. 1627 (IMO 2020). A description of the current state of the method is available from Shigunov (2023). Anastopoulos and Spyrou (2022, 2023b) have presented a formal argument on the equivalency between the extrapolation over the wave heights and the critical wave group method. Moreover, they have proposed and evaluated two improved formulae for extrapolation which retain the simple character of the original. Completing this comprehensive introduction, the authors would like to refer the reader to a comparative review of some of the described approaches, available in Wandji (2023).

1.8. Objective and structure of the paper

The objective of this paper is rather simple – to estimate probability of capsizing from relatively short numerical simulations without observing the event. The paper is a two-fold: study condition of capsizing with a Reduced-Order Model (ROM) and then apply this knowledge to engineering-level numerical simulation of ship motions in waves.

A single-degree-of-freedom dynamical system with piecewise linear restoring is used as a ROM. The study of the ROM includes:

- Demonstration that the ROM can model capsizing as transition to another equilibrium,
- Demonstration that the ROM is qualitatively valid in terms of roll motions,
- What are the conditions of capsizing and how to compute probability of capsizing in the simplest case?
- How to include influence of wind and stability variation in waves?
- Formulation of the lessons learned from ROM.

Then the paper goes further into numerical applications of these "lessons learned":

- Formulation of a metric of likelihood of capsizing in a numerical dynamical system incorporating body-nonlinear formulation for hydrostatic and Froude-Krylov forces.
- Study of extreme-value properties of the metric of likelihood of capsizing.
- Completion of the estimate for probability of capsizing and numerical examples.

2. Piecewise linear system revisited

2.1. Dynamical system without damping or excitation

As capsizing is a transition to motion at the upside-down stable equilibrium (Fig. 1), a qualitative mathematical model of capsizing should include at least three equilibria: two stable and one unstable. Belenky (1989) considered a basic reduced-order model (ROM): a dynamical system with natural frequency ω_ϕ and a piecewise linear restoring $f^*(\phi)$, shown in Fig. 2.

$$\ddot{\phi} + \omega_\phi^2 f^*(\phi) = 0 \tag{4}$$

where:

$$f^* = \begin{cases} k_2(\phi + \phi_{m1}) + k_1(\phi - \phi_{m0}) - \phi_{m0}; & \phi < -\phi_{m1} \\ -k_1(\phi + \phi_{m0}) - \phi_{m0}\ ; & -\phi_{m1} \le \phi < -\phi_{m0} \\ \phi\ ; & -\phi_{m0} \le \phi \le \phi_{m0} \\ -k_1(\phi - \phi_{m0}) + \phi_{m0}\ ; & \phi_{m0} < \phi \le \phi_{m1} \\ k_2(\phi - \phi_{m1}) - k_1(\phi - \phi_{m0}) + \phi_{m0}\ ; & \phi_{m1} < \phi \end{cases} \tag{5}$$

The slope coefficients for the piecewise linear terms k_1 and k_2 are defined as:

$$k_1 > 0\ ;\ k_2 = \frac{k_1(\phi_{m1} - \phi_{m0}) - \phi_{m0}}{\pi - \phi_{m1}} \tag{6}$$

The solution for the ordinary differential equation (4) for the range 0 ($-\phi_{m0} \le \phi \le \phi_{m0}$) and range 1 ($\phi_{m0} < \phi \le \phi_{m1}$) is expressed as:

$$\phi = \begin{cases} C_1\ cos\big(\omega_\phi(t - t_{m0})\big) + C_2\ sin\big(\omega_\phi(t - t_{m0})\big); \\ -\varphi_{m0} \le \varphi \le \varphi_{m0} \\ A{\cdot}exp\Big(\omega_\phi\sqrt{k_1}\,(t - t_{m1})\Big) + B{\cdot}exp\Big(-\omega_\phi\sqrt{k_1}\,(t - t_{m1})\Big) + \phi_v; \\ \phi_{m0} < \phi \le \phi_{m1} \end{cases} \tag{7}$$

The solutions for other ranges are similar. The arbitrary constants depend on the initial conditions at the range 0 ($\phi_0;\ \dot{\phi}_0$), taken at the time instant t_{m0}, and range 1 ($\phi_1;\ \dot{\phi}_1$), taken at the time instant t_{m1}:

$$C_1 = \phi_0\ ,\quad C_2 = \frac{\phi_0}{\omega_\varphi}$$
$$A = \frac{\dot{\phi}_1 + \omega_\varphi\sqrt{k_1}(\phi_1 - \phi_v)}{2\omega_\varphi\sqrt{k_1}} \tag{8}$$
$$B = -\frac{\dot{\phi}_1 - \omega_\phi\sqrt{k_1}(\phi_1 - \phi_v)}{2\omega_\varphi\sqrt{k_1}}$$

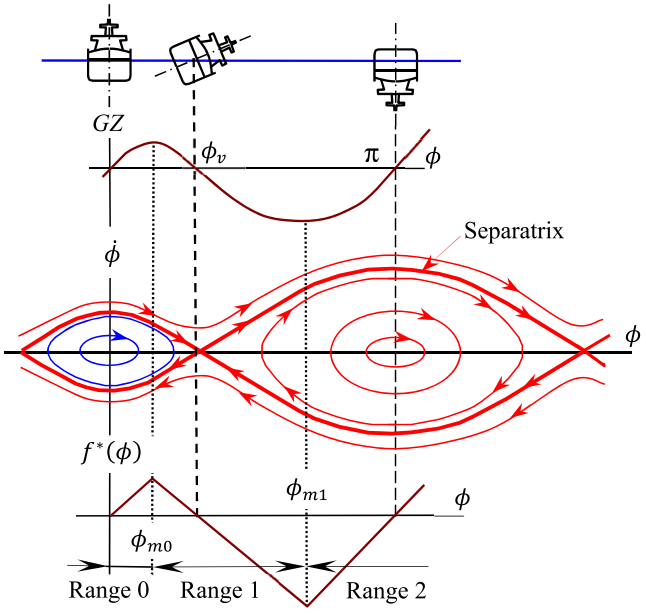

Fig. 2. Phase plane topology of capsize and piecewise linear stiffness (Belenky, 1993).

where ϕ_v is the position of unstable equilibrium:

$$\phi_v = \phi_{m0}\frac{k_1+1}{k_1} \tag{9}$$

The solution (7) in range 1 contains an exponent with a positive argument. The sign of the arbitrary constant A defines the path of the solution. A transition to the range 2 in Fig. 2 will be followed by an attraction to the stable equilibrium at $\pm\pi$, which means capsizing. The conditions for the transition are:

$$\begin{aligned}&(\phi_{m0} < \phi \le \phi_{m1}) \cap (A > 0) \Rightarrow \phi \to \pi\\ &(-\phi_{m1} \le \phi < -\phi_{m0}) \cap (A < 0) \Rightarrow \phi \to -\pi\end{aligned} \tag{10}$$

As the equilibrium transition problem in the unbiased dynamical system is symmetrical, only capsizing to starboard (through positive side) is examined further. Consider an instant of crossing into the range 1 in Fig. 2. The value of the roll rate at the instant of upcrossing ϕ_{m0} that leads to capsizing is the critical roll rate and is computed from the condition $A > 0$:

$$\dot{\phi}_{cr} = -\omega_\phi\sqrt{k_1}(\phi_{m0} - \phi_v) \tag{11}$$

The dynamical system (4) does model the transition to another stable equilibrium, but does not model attraction to this other equilibrium. From the phase plane in Fig. 2, the dynamical system is expected to show rotation upon crossing of the separatrix.

2.2. Damped system without excitation

To model a transition with further attraction to the capsized equilibrium (Fig. 3), damping should be added to the dynamical system (4):

$$\ddot{\phi} + 2\delta\dot{\phi} + \omega_\phi^2 f^*(\phi) = 0 \tag{12}$$

where δ is a damping coefficient. The conditions of capsizing are expressed via critical roll rate at the instant of upcrossing of the boundary ϕ_{m0}:

$$\dot{\phi}_{cr} = -\left(\delta + \sqrt{k_1\omega_\phi^2 + \delta^2}\right)(\phi_{m0} - \phi_v) \tag{13}$$

2.3. Damped system with periodic excitation

To model capsizing in waves, excitation is added to the dynamical system (12):

$$\ddot{\phi} + 2\delta\dot{\phi} + \omega_\phi^2 f^*(\phi) = \alpha\sin(\omega t) \tag{14}$$

where α is an amplitude and ω is the frequency of the wave excitation. The condition for capsizing at the boundary crossing instant is modified with the values of a particular solution p_1 and its derivative $\dot{p}_1$ at range 1:

$$\dot{\phi}_{cr} = -\left(\delta + \sqrt{k_1\omega_\phi^2 + \delta^2}\right)(\phi_{m0} - \phi_v - p_1) + \dot{p}_1 \tag{15}$$

$$p_1 = p_a\cos\varphi_1, \quad \dot{p}_1 = -p_a\omega\sin\varphi_1, \tag{16}$$

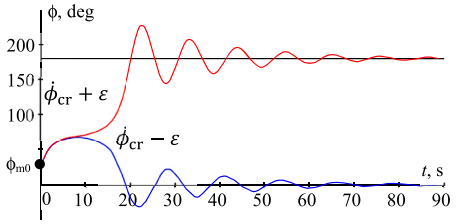

Fig. 3. Capsizing modeled with a dynamical system with piecewise linear restoring and damping without excitation ($\phi_{m0} = 0.5$ rad, $\phi_{m1} = 2.5$ rad, $k_1 = 0.7$ rad s, $\omega_\phi = 0.5$ rad/s, $\delta = 0.05$ 1/s; ε is a small value, $\varepsilon = 10^{-3}$).

$$p_a = \frac{\alpha}{\sqrt{\left(\omega^2 + k_1\omega_\phi^2\right)^2 + 4\omega^2\delta^2}}$$
$$\varphi_1 = \arctan\frac{2\omega\delta}{\omega^2 + k_1\omega_\phi^2} \tag{17}$$

Examples of capsizing and non-capsizing time histories are shown in Fig. 4.

The dynamical system with piecewise linear restoring (14) models capsizing as a transition to motion around another stable equilibrium and provides a simple formulae for the conditions of capsizing. In order to determine whether the dynamical system (14) is a qualitatively correct description of a ship rolling in waves, its ability to reproduce known properties from other models of large-amplitude roll motions is investigated in Section 2.4.

2.4. Period of free oscillations, fold bifurcation and other nonlinear properties of roll

A period of large free roll motion is known to be dependent on the initial roll angle (e.g., Section 4.1.1 of Belenky and Sevastianov 2007). The dynamical system (4) has this property: a period of its free motions depends on the initial displacement for $\varphi > \varphi_{m0}$ (Belenky, 1995):

$$T_\phi(\phi_0) = \frac{4}{\omega_\phi\sqrt{k_1}}\left(\frac{1}{\sqrt{k_1}}\operatorname{arcosh}\frac{\phi_v - \phi_{m0}}{\phi - \phi_0}\right.$$
$$\left.+\arctan\frac{\phi_{m0}\omega_\phi}{\omega_\phi\sqrt{k_1}\sqrt{(\phi_v - \phi_{m0})^2 - (\phi_v - \phi_0)^2}}\right) \tag{18}$$

The derivation of formula (18) can also be found in Section 4.1.2 of Belenky and Sevastianov (2007). This dependence is depicted in Fig. 5 in a form of the backbone curve. It bends left, showing soft-nonlinearity of restoring, which is consistent with the shape of the piecewise linear restoring term.

The amplitude of the steady state solution near the upright equilibrium can be approximated with an equivalent linearization using the backbone curve (18), see Belenky (2000):

$$\phi_a = \frac{\alpha}{\sqrt{\left(\omega^2 - (\omega_B(\phi_a))^2\right)^2 + 4\omega^2\delta^2}}$$
$$\Downarrow \tag{19}$$
$$\omega(\phi_a) = \sqrt{(\omega_B(\phi_a))^2 - 2\delta^2 \pm \sqrt{D(\phi_a)}}$$

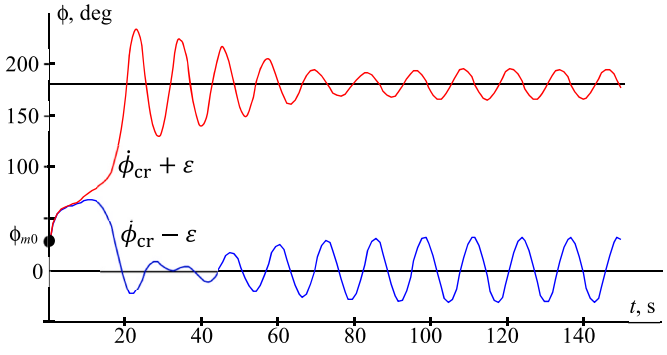

Fig. 4. Capsizing modeled with a dynamical system with piecewise linear restoring and damping with excitation ($\omega = 0.5$ 1/s, $\alpha = 0.0288$ rad; ε is a small value, $\varepsilon = 10^{-3}$, other parameters are same as in Fig. 3).

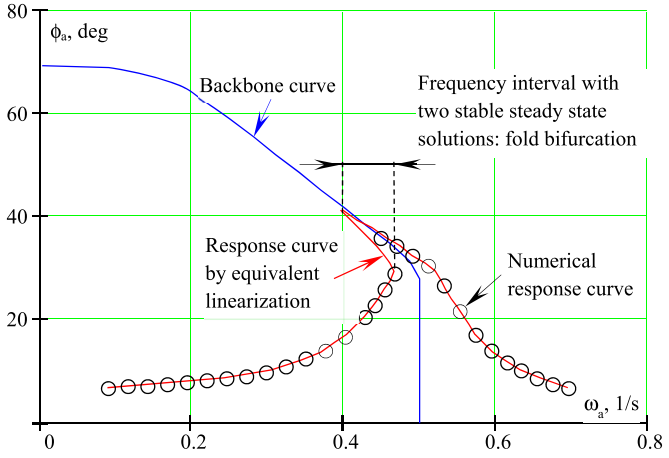

Fig. 5. Dynamical system with piecewise linear restoring ($\varphi_{m0} = 0.5$ rad, $\varphi_{m1} = 2.5$ rad, $k_1 = 0.7$ rad s, $\omega_\phi = 0.5$ rad/s), backbone and response curves for $\delta = 0.05$ 1/s and $\alpha = 0.0288$ rad.

$$D(\phi_a) = \left(\frac{\alpha}{\phi_a}\right)^2 - 4\delta^2\left((\omega_B(\phi_a))^2 - \delta^2\right)$$

$$\omega_B(\phi_a) = \frac{2\pi}{T_\phi(\phi_a)} \tag{20}$$

The response curve approximated with equivalent linearization (19, 20) is shown in Fig. 5. Its shape indicates the existence of a frequency interval where three steady-state solutions are possible: two stable ones separated by an unstable one. The unstable steady-state solution cannot be realized for any appreciable time either numerically or physically. The choice between the two stable steady-state solutions is determined by initial conditions. This phenomenon is known as fold bifurcation, and has been extensively studied in nonlinear dynamics and observed in model tests (Francescutto et al., 1994).

The response curve, computed by the numerical integration of equation (14) is shown in Fig. 5, confirming the existence of two stable steady state solutions. Calculations were performed for two sequences of excitation frequencies from high-to-low and low-to-high. Once the solution is stabilized, the steady state values (roll angle, roll rate and time of sampling) were the initial conditions for the next frequency. The frequency interval of fold bifurcation, obtained numerically, is somewhat smaller compare to the one, shown by equivalent linearization. A possible reason for this is that the unstable solution is too close to the large-amplitude stable steady-state solution, leading to numerical accuracy issues.

The characteristics of a steady-state solution of a dynamical system with piecewise linear restoring can be accurately computed with a semi-analytical technique, as described in Belenky (2000). The values of roll rate at the instant of crossing the boundary $\pm\phi_{m0}$ are found as well as the time of these crossings, conditioned by the motion period being equal to the excitation period. This results in a system of five nonlinear algebraic equations, which can be solved numerically. Once these elements of steady-state solution are found, the amplitude is computed numerically. The technique also produces motion stability indicators: eigenvalues and trace-determinant of the Jacobian matrix (Section 4.4.4 of Belenky and Sevastianov, 2007). While this semi-analytical technique did provide the required answers, continuation methods would be more computationally efficient and accurate (see e.g., Spyrou and Tigkas, 2007).

The motion stability analysis of the piecewise linear system (Belenky, 2000) has proven that the frequency interval with multiple steady state solutions, depicted in Fig. 5, is associated with an escape of the eigenvalues through the positive direction, characteristic of a fold bifurcation. Flip bifurcation was also observed leading to deterministic chaos through period doubling. Essentially, the dynamical system with piecewise linear restoring demonstrates a bifurcation behavior similar to a typical qualitative model of nonlinear ship motions, e.g. Duffing equation with softening restoring see Section 4.5 of (Belenky and Sevastianov, 2007).

Another important property of a dynamical system, relevant to large-amplitude roll and capsizing, is the fractal erosion of the safe basin (e.g., Rainey et al., 1990). The dynamical system with piecewise linear restoring does have this property as well (Belenky, 2000), leading to the conclusion that the piecewise linear system (14) is as valid qualitative model of large-amplitude roll motion, as a dynamical system with "smooth" restoring.

The main advantage of the dynamical system with piecewise linear restoring is its ability to identify imminent capsizing at the instant of the crossing of the boundary $\pm\phi_{m0}$. It seems not to provide any computational advantages for the characterization of the entire motion, compared to a conventional numerical solution of ordinary differential equation. Essentially, dynamical system with piecewise linear restoring should be considered as a reduced-order model (ROM) for capsizing as a transition to another stable equilibrium see also (Weems et al., 2022).

2.5. Random excitation and conditions of capsizing

Calculation of probability of capsizing as a rare transition to another stable equilibrium in a piecewise linear dynamical system was recently revisited in Belenky et al. (2016). It is briefly reviewed here in order to remind the reader of the principal ideas. Consider the dynamical system (14) under stochastic excitation:

$$\ddot{\phi} + 2\delta\dot{\phi} + \omega_\phi^2 f^*(\phi) = \alpha_e(t) \tag{21}$$

where $\alpha_e(t)$ is modeled with Fourier series:

$$\alpha_e(t) = \sum_{i=1}^{N} \alpha_{ei} \sin(\omega_i t + \varphi_{0i}) \tag{22}$$

The amplitudes α_{ei} are determined from a spectrum, discretized with N frequencies ω_i, while φ_{0i} are random phase shift angles, uniformly distributed from 0 to 2π.

Capsizing becomes a random event when the roll angle upcrosses the boundary ϕ_{m0} while the roll rate at the upcrossing time instant $\dot{\phi}_1$ exceeds the critical roll rate (15). Considering the capsizing as Poisson process (1), its rate can be presented as:

$$r_C = r_U(\phi_{m0})P(\dot{\phi}_1 > \dot{\phi}_{cr}) \tag{23}$$

where $r_U(\phi_{m0})$ is the rate of upcrossing of the boundary ϕ_{m0} and P stands for probability.

Equation (23), which first appeared in Belenky (1989), expresses an important concept of separating the evaluation of the probability of rare event into two problems. The first problem, identified as the "non-rare" problem, is the calculation of the rate of upcrossing $r_U(\phi_{m0})$ over the boundary ϕ_{m0}. The second problem, identified as the "rare" problem, is determining which of these upcrossings will lead to capsizing, i.e., the calculation of the probability $P(\dot{\phi}_1 > \dot{\phi}_{cr})$.

The idea to consider non-rare and rare problems separately is, essentially, not new. The concept of the tail of the distribution that is treated separately (e.g., Pickands, 1975) can be interpreted that way. Rarity of roll motion however also means a difference in physics caused by nonlinearity, which was implied in the term "principle of separation", introduced in Belenky et al. (2012). Mohammad et al. (2016) independently pursue a similar idea in their probabilistic decomposition-synthesis method.

2.6. Non-rare problem: boundary upcrossing

In the absence of capsizing, the upcrossing of the boundary ϕ_{m0} is

assumed rare and the dynamical system (21) does not spend much time above the boundary ϕ_{m0}. Ordinary differential equation (21) is linear within the intervals $-\phi_{m0} \le \phi \le \phi_{m0}$ and $\pm\phi_{m0} < \phi \le \pm\phi_{m1}$. Every time the boundary $\pm\phi_{m0}$ is crossed, a general solution of homogenous equation is generated. For the interval $-\phi_{m0} \le \phi \le \phi_{m0}$, this solution is a decaying oscillation with the frequency $\omega_{\phi g}$ (as external forcing is not included in the homogenous equation). The general solution at the interval $\pm\phi_{m0} < \phi \le \pm\phi_{m1}$ is a sum of two exponential functions of time. Thus, the influence of general solutions on the distribution and its moments can be neglected, so the distribution of roll angles and rates can be assumed normal. As the system (21) is linear below ϕ_{m0}, the rate of upcrossings $r_U(\phi_{m0})$ is expressed as:

$$r_U(\phi_{m0}) = \frac{1}{2\pi}\sqrt{\frac{V_{\dot\phi}}{V_\phi}}\exp\left(-\frac{\phi_{mo}^2}{2V_\phi}\right) \tag{24}$$

where V_ϕ and $V_{\dot\phi}$ are variances of roll angles and rates, respectively, which can be computed in the frequency domain, see equation (32) in subsection 2.9.

2.7. Rare problem: distribution of roll rate at upcrossing

The distribution of roll rates at the instant of upcrossing $\dot\phi_1$ is a bit more subtle problem than it may appear. Belenky (1989, 1993) assumed a folded normal distribution for $\dot\phi_1$, arguing that as roll angles and rates are independent, upcrossing can occur with any positive roll rate. The fallacy of this argument is that while roll angles and rates are independent when sampled simultaneously at a random moment, the upcrossing is a particular moment, conditioned not only by positivity of the rate $\dot\phi_1 > 0$ but also by crossing the boundary $\phi = \phi_{m0}$. As a result, the value of roll rate at the instant of upcrossing follows Rayleigh distribution, see e.g., p. 201 of (Leadbetter et al., 1983). An abridged derivation is also available from (Belenky et al., 2016):

$$\mathrm{PDF}(\dot\phi_1) = \frac{\dot\phi_1}{V_{\dot\phi}}\exp\left(-\frac{\dot\phi_1^2}{2V_{\dot\phi}}\right) \tag{25}$$

The Rayleigh distribution (25) is applicable to roll rate samples at all observed upcrossings. The process of roll motions has a relatively narrow spectrum and a typical decorrelation time is on the order of 1 min. That means that an upcrossing of the boundary ϕ_{m0} will be likely followed by one or more upcrossings at the subsequent periods. Thus, upcrossing events are likely to appear in clusters. The distribution of the roll rate at the instant of a particular upcrossing in such a cluster may be different from (25). For example, the distribution of the roll rate at the first upcrossing in a cluster has a shape of Rayleigh distribution, but its parameter is different from $V_{\dot\phi}$ (Belenky et al., 2019).

While the upcrossings through the boundary ϕ_{m0} may not always follow Poisson flow, due to clustering, the dependence of capsizing events is of no concern, as it can occur only once in a record. As a result, Rayleigh distribution (25) can be applied for the roll rate values at the instant of upcrossing without limitations.

2.8. Rare problem: difference between instantaneous and critical roll rate

The difference between the instantaneous and critical roll rates is an indicator of the likelihood of capsizing. The roll rate at the instant of upcrossing $\dot\phi_1$ is not the only random quantity in the rare problem $P(\dot\phi_1 > \dot\phi_{cr})$. The critical roll rate $\dot\phi_{cr}$ (equation 15) is a deterministic function of two random variables p_0 and $\dot p_0$. The condition of capsizing after upcrossing in irregular wave is expressed as the difference of two random quantities:

$$\dot\phi_1 - \dot\phi_{\mathrm{cr}} = \dot\phi_{\mathrm{d}} > 0 \tag{26}$$

where $\dot\phi_d(t)$ is the process of the difference between the instantaneous and critical roll rate:

$$\dot\phi_{\mathrm{d}}(t) = \left(\delta + \sqrt{k_1\omega_\phi^2 + \delta^2}\right)(\phi_{\mathrm{m0}} - \phi_v - p(t)) + \dot\phi(t) - \dot p(t) \tag{27}$$

Formally, the process $\dot\phi_d(t)$ can be evaluated at any instant of time. However, it is relevant to capsizing only at the instant of upcrossing of the boundary ϕ_{m0}. Following Belenky et al. (2011), the condition of capsizing (26) can be re-written as:

$$(\dot\phi_d(t) > 0) \cap (\phi(t) = \phi_{\mathrm{m0}}) \cap (\dot\phi(t) > 0) \tag{28}$$

Calculation the probability of capsizing after upcrossing requires evaluation of the probability of a positive value of the process $\dot\phi_d(t)$ when another process $\phi(t)$ up-crosses the boundary ϕ_{m0}, while the processes $\dot\phi_d(t)$ and $\phi(t)$ are dependent. The distribution of $\dot\phi_d(t)$ is expressed as follows, see e.g., Section 8.3 of (Lindgren, 2013) or pp. 161–162 of (Sólnes, 1997); abridged simplified derivation is available in Appendix to (Belenky et al., 2011):

$$\mathrm{PDF}(\dot\phi_d) = \frac{\int_0^\infty \dot\phi\cdot\mathrm{PDF}(\phi = \phi_{\mathrm{m0}}, \dot\phi, \dot\phi_d)d\dot\phi}{\int_0^\infty \dot\phi\cdot\mathrm{PDF}(\phi = \phi_{\mathrm{m0}}, \dot\phi)d\dot\phi} \tag{29}$$

The process $\dot\phi_d(t)$ is a linear function of three other processes: roll rate $\dot\phi(t)$, the particular solution in range 1 $p(t)$ and its derivative $\dot p(t)$. The process of roll rates $\dot\phi(t)$ is assumed normal (due to small time spent beyond the boundary ϕ_{m0}), while the particular solution $p(t)$ and its derivative $\dot p(t)$ are normal as the dynamical system is linear within range 1. Thus, $\dot\phi_d(t)$ is also normal and the evaluation of (29) should be possible.

The derivation of the PDF (29) is available from Glotzer et al. (2024) and the reader is referred to that work for the complete argument, leading to the following result (using the nomenclature of the cited source):

$$\mathrm{PDF}(\dot\varphi_d) \propto exp\left(-\frac{C_0}{2}\right) \times\left[1 + \sqrt{\pi}\ \frac{B_0}{\sqrt{A_0}}\ exp\left(\frac{B_0^2}{A_0}\right)\left(erf\left(\frac{B_0}{\sqrt{A_0}}\right) - 1\right)\right] \tag{30}$$

where A_0 is a constant, B_0 is a linear function of $\dot\phi_d$ and C_0 is a quadratic function of $\dot\phi_d$, while:

$$\mathrm{erf}(x) = \frac{2}{\sqrt{\pi}}\int_0^x \exp(-u^2)du$$

The tail of the distribution (30) is exponential, as shown by Glotzer et al. (2024).

2.9. Simplified rare problem

Equation (27) can be significantly simplified if the particular solution $p(t)$ and its derivative $\dot p(t)$ are assumed small. The particular solution $p(t)$ describes a response of the dynamical system to external forcing in the range 1, i.e., from the maximum of a restoring function to its minimum; the derivative of the restoring function is negative and the system is a repeller. Therefore, resonance is absent in range 1, see the amplitude of the particular solution $p(t)$ in Fig. 6 (Belenky, 1989, 1993).

This absence of resonance leads to:

$$\mathrm{V}_{\dot\phi} \gg \mathrm{V}_{\dot p} \text{ and } \mathrm{V}_{\dot\phi} \gg \left(\delta + \sqrt{k_1\omega_\phi^2 + \delta^2}\right)^2 \mathrm{V}_p \tag{31}$$

where $\mathrm{V}_{\dot\phi}, \mathrm{V}_p$ and $\mathrm{V}_{\dot p}$ are the variances of roll rates, the particular solution in range 1, and its derivative, respectively:

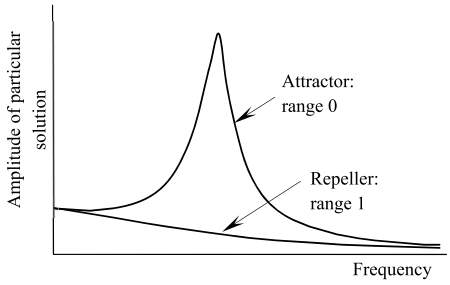

Fig. 6. Amplitudes of particular solutions in frequency-domain (Belenky et al., 2008).

$$V_{\dot{\phi}} \approx 0.5\sum_{i=1}^{N}\frac{\alpha_{ei}^2\omega_i^2}{\left(\omega_i^2-\omega_\phi^2\right)^2+4\omega_i^2\delta^2} \tag{32}$$

$$V_{p} = 0.5\sum_{i=1}^{N}\frac{\alpha_{ei}^2}{\left(\omega_i^2+k_1\omega_\phi^2\right)^2+4\omega_i^2\delta^2} \tag{33}$$

$$V_{\dot{p}} = 0.5\sum_{i=1}^{N}\frac{\alpha_{ei}^2\omega_i^2}{\left(\omega_i^2+k_1\omega_\phi^2\right)^2+4\omega_i^2\delta^2} \tag{34}$$

Assuming that the covariance between these processes is also small, the particular solution and its derivative in range 1 can be treated as deterministic and be substituted by their means, which are zeros. As a result, the critical roll rate $\dot{\phi}_{\mathrm{cr}}$ becomes a constant (13) and the difference between the instantaneous and the critical roll rate becomes a function of a single random argument $\dot{\phi}$ and is expressed as:

$$\dot{\phi}_d(t) = \dot{\phi}(t) + \left(\delta+\sqrt{k_1\omega_\phi^2+\delta^2}\right)(\phi_{\mathrm{m0}}-\phi_v) \tag{35}$$

The PDF of $\dot{\phi}_{\mathrm{d}}$ becomes a shifted Rayleigh distribution:

$$\mathrm{PDF}(\dot{\phi}_d) = \frac{\dot{\phi}_d+\dot{\phi}_{cr}}{V_{\dot{\phi}}}\exp\left(-\frac{\left(\dot{\phi}_d+\dot{\phi}_{cr}\right)^2}{2V_{\dot{\phi}}}\right) \tag{36}$$

The assumption of the negligibility of the particular solution $p(t)$ and its derivative $\dot{p}(\mathrm{t})$ is equivalent to the case of "no excitation above the boundary ϕ_{m0}" considered in Belenky et al. (2019) for the structure of the tail of the response distribution. The tail of the distribution (36) is exponential, similar to the case with the complete solution (30) – tail of Rayleigh distribution is known to be exponential.

The application of the method with "no excitation above the boundary ϕ_{m0}" was executed by Iskandar et al. (2000, 2001) and Iskandar and Umeda (2001, 2001a). Folded normal distribution was used for the roll rate at upcrossing, as the error in (Belenky, 1989, 1993) was not found until (Belenky et al., 2008). Nevertheless, the numerical results seem to be reasonable (probability estimates were believable) – most likely because a folded normal distribution also has an exponential tail and is able to recover the correct behavior for small probabilities.

2.10. Influence of wind

The piecewise linear dynamical system (21) can model capsizing under the action of gusty wind along with irregular waves. This was implemented through a modification of the excitation: adding a mean value and changing its variance. The model in (Belenky, 1994) includes roll and sway, but the coupling is incomplete as the influence of roll on sway was not included:

$$\begin{cases}(M+A_{22})\ddot{\eta}+R_{D\eta}(\dot{\eta}) = F_{w\eta}(t)+F_{a\eta}(t)\\ (I_x+A_{44})\ddot{\phi}+B_{44}\dot{\phi}+\rho g\nabla\cdot GZ(\phi)+A_{42}\ddot{\eta}+M_{D\eta}(\dot{\eta})\\ \qquad = M_{w\eta}(t)+M_{a\eta}(t)\end{cases} \tag{37}$$

where η is horizontal displacement, i.e., sway and drift motion (understanding sway as a periodic component and drift as a slowly changing mean of this periodic component), M is the mass of the ship, A_{22} and A_{42} are sway-sway and sway-roll added masses, respectively, $R_{D\eta}(\dot{\eta})$ and $M_{D\eta}(\dot{\eta})$ are the drag force in sway direction and its moment, $F_{w\eta}(t)$ and $M_{w\eta}(t)$ are the Froude-Krylov wave force and its moment, while $F_{a\eta}(t)$ and $M_{a\eta}(t)$ are the aerodynamic (wind) force and its moment.

The aerodynamic (wind) force is modeled as a stationary stochastic process with a non-zero mean value corresponding to the mean wind velocity. The latter is considered to be large in comparison with the sway and drift velocity $\dot{\eta}$. A quadratic form is assumed for the drag force $R_{D\eta}(\dot{\eta})$. It is further linearized at the mean wind speed, leaving the GZ curve as the only nonlinearity in (37), which is modeled with the piecewise linear term (5). The sway equation in (37) becomes linear and produces a closed-form solution for the sway/drift velocity $\dot{\eta}$. The sway/drift velocity and its derivative $\ddot{\eta}$ are substituted into the roll equation (37) and become a part of the excitation, which is also modified by the wind moment $M_{a\eta}(t)$. As a result, the excitation has a mean value, corresponding to the mean wind velocity.

Belenky (1994) modified the simplified solution for the rare problem. The particular solution was substituted by its mean value, leading to the following formula for the difference between the instantaneous and critical roll rate:

$$\dot{\phi}_d(t) = \dot{\phi}(t) + \left(\delta+\sqrt{k_1\omega_\phi^2+\delta^2}\right)(\phi_{\mathrm{m0}}-p_m-\phi_v) \tag{38}$$

where p_m is a mean value of the particular solution $p(t)$, reflecting steady drift.

Paroka et al. (2006) provided a complete solution for the rare problem, including the influence of $p(t)$ and its derivative on $\dot{\phi}_{\mathrm{d}}(t)$, which is referred to as an "exact method" in the cited source. A comparison between the exact and simplified method shows little difference, though the simplified method appears to be more conservative for smaller mean wind velocities. Paroka et al. (2006) includes a study of a number of other influences and proposes an alternative simplification, which is to keep the derivative of the particular solution $\dot{p}(\mathrm{t})$ but substitute $p(t)$ with its mean value:

$$\begin{aligned}\dot{\phi}_d(t) = &\left(\delta+\sqrt{k_1\omega_\phi^2+\delta^2}\right)(\phi_{\mathrm{m0}}-p_m-\phi_v)\\ &+\dot{\phi}(t)-\dot{p}(t)\end{aligned} \tag{39}$$

Paroka and Umeda (2006) compared the solution (39) with the method by Bulian and Francescutto (2004) and a Monte-Carlo numerical simulation. The piecewise linear solution underpredicts the probability of capsizing, especially for large values of the mean wind velocity. As the problem with folded normal distribution of the roll rate at the instant of upcrossing was not found until Belenky et al. (2008), the application of folded normal PDF was likely to be responsible for this underprediction.

2.11. Influence of variation of stability of waves

Attempts have been made to include the effect of stability variation in waves into the piecewise linear model. Belenky (1997) applied an empirical method by Nechaev (1989) to account for variation on GZ curve; English description of this empirical method is available from (Belenky and Sevastianov, 2007). The method provides an amount of variation in the GZ curve at a given angle when a midship section is located near the crest or the trough of a regular wave. A wave pass was modeled with a random phase, while appropriate distributions were intended to be used for the wave heights and lengths. Different distributions for the external excitation and stability variation were used.

The main disadvantage of this idea is that the dynamics of roll motion with variable stiffness is not included in the model. This feature is important, as the variation of stiffness occurs at the same time scale as the motions, see e.g., Spyrou (2009). Another important missing feature

is the influence of surging, which may "modulate" the stability variations (Umeda et al., 1990; Umeda and Yamakoshi, 1994).

The most obvious answer to this challenge is to model the variation of stability with the piecewise linear term, making it two-dimensional, as illustrated in Fig. 7. The maximum GZ point and the angle of vanishing stability, which define the piecewise linear term, become stochastic processes. Proper dynamics of roll motions can be modeled with this approach, as shown in Belenky (2000a). However, the solution becomes numerical and loses all of the advantages of the closed-form expressions (30) and (36).

The closed-form solution still can be derived if the decreasing part of the stiffness remains parallel to itself, as shown in Fig. 8 (Belenky et al., 2011). The influence of the stability variation is included in a particular solution in range 1, so the simplified solution (31) is no longer applicable. The non-rare problem is formulated for upcrossing of the process of the difference between the roll angle and $\phi_{m0}(t)$. The rare problem leads to distribution (30). The stability variation in waves is reflected in the parameters of the distribution but does not affect its exponential tail.

Belenky et al. (2011) describe a comparison between the closed-form piecewise linear expression for the rate of capsizing against an estimate from time-domain numerical integration of the differential equation with variable piecewise linear restoring. While the comparison was limited, the analytical and numerical results were shown to agree, insofar as the former was included in the confidence interval of the latter. This can be considered as an indirect confirmation that the incorrect distribution of roll rate at upcrossing may be the reason for inconsistencies reported by Paroka and Umeda (2006).

To model the stability variation in waves, Belenky and Weems (2008a) developed a method for the calculation of the instantaneous GZ curve within a potential-flow time-domain simulation. The idea is to "freeze" the free surface, incline a ship to an angle from its instantaneous position and balance it in pitch and heave. The residual roll moment yields a value for the instantaneous GZ curve at the angle the ship was inclined to. The method was implemented in the potential-flow seakeeping code LAMP (Large-Amplitude Motion Program), see e.g., (Shin et al., 2003) and was used for a statistical analysis of the elements of the instantaneous GZ curve: transverse metacentric height (GM), angle of vanishing stability, maximum GZ and its corresponding angle. Modeling distributions of these elements encountered significant difficulties and does not seem to be practical.

LAMP simulations also revealed a complex relationship between roll angles and rates in stern quartering seas when stability variations are significant. As a stationary stochastic process and its temporal derivative, roll angles and rates are not correlated. However, the absence of correlation infers independence only for Gaussian processes. Belenky and Weems (2019) reported that roll angles and rates in stern quartering seas are dependent, while uncorrelated. The dependence can be revealed through higher-order moments. This dependence may have significant influence on both the rare and non-rare problems.

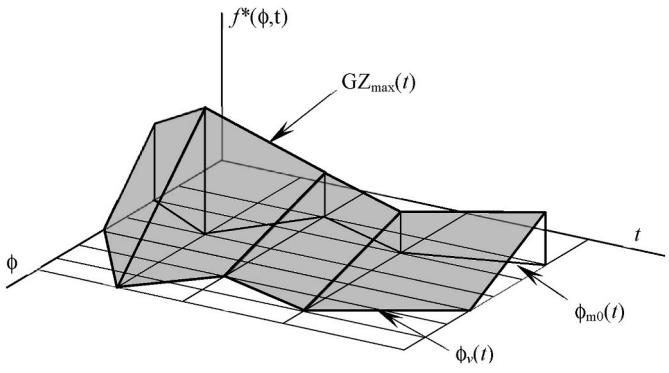

Fig. 7. Time-dependent piecewise linear term describing decreasing part of the stiffness (Belenky, 2000a).

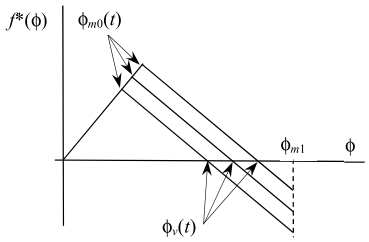

Fig. 8. Time-dependent piecewise linear term describing decreasing part of the stiffness, allowing a closed-form solution (Belenky et al., 2011).

2.12. Role of analytical solutions

An obvious practical advantage of a closed-form solution is its potential for stability criterion. Close-form solutions are easy to implement even if they use a non-elementary function. Even semi-analytical solution, containing numerical integration or requiring numerical solution of algebraic equation, are attractive as criteria as the results of these numerical calculations are easily verifiable in most cases. That is probably a reason why Paroka and Umeda (2006) considered practical ways to present the GZ curve with a piecewise linear term. If sufficiently developed and validated, a piecewise linear solution for capsizing probability could represent a probabilistic alternative to the weather criterion as well as a linearization method by Bulian and Francescutto (2004).

While the method by Bulian and Francescutto (2004) was included into the IMO Interim Guidelines of the Second Generation Intact Stability Criteria MSC.1/Circ. 1627 (IMO, 2020), it is not a probabilistic alternative to the weather criterion. The reason is that a probabilistic criterion is not consistent with the weather criterion, see e.g., Peters and Belenky (2023). As a result, the weather criterion cannot naturally "evolve" into a probabilistic criterion.

The limited practical applicability of the piecewise linear model justifies the redirection of research regarding the estimation of capsizing probabilities towards numerical approaches. Nonetheless, several important results were achieved in the course of the study of piecewise linear dynamical system:

- Capsizing can be considered as a combination of two problems: non-rare and rare. The non-rare problem is the upcrossing of an intermediate level, while the rare problem is determination of the condition of capsizing if the intermediate level has been crossed.
- The non-rare problem allows use of Poisson flow to model capsizing and provides relation between probability and time.
- The condition of capsizing can be expressed as a critical roll rate at the instant of roll upcrossing of an intermediate level.
- The critical roll rate is a random variable taking different values at each upcrossing. The variation of stability in waves may have a significant contribution in the variability of the critical roll rate.
- The difference between an instantaneous and critical roll rate, computed at the instant of upcrossing, can be used as a metric of likelihood of capsizing.
- The distribution of the differences between the instantaneous and critical roll rates is likely to have an exponential tail.

3. Numerical approach: split-time method

3.1. Body-nonlinear formulation

One significant assumption used for derivation of equation (2) is the separation of the hydrostatic and Froude-Krylov forces. This artificial technique is needed to formulate the roll motion problem into an ordinary differential equation in which all the terms are explicit functions that can be approximated with closed-form expressions. This technique

allows the roll motion problem to be brought into the domain of the theory of oscillators and helps to find the most important qualitative relationships between external forces and the roll response.

With the advance of seakeeping simulation codes and computational resources, one degree-of-freedom (1-DOF) roll models like (2) have transitioned from being an engineering tools towards a reduced-order model (ROM) used to guide the development of multiple-DOF numerical methods that are free of most of the assumptions and limitations, imposed to derive the 1-DOF models. One of the most important advantages of the multiple-DOF numerical methods is the incorporation of a body-nonlinear formulation, which manifests itself as an inseparability of the hydrostatic restoring and Froude-Krylov forces.

A core implementation of the body-nonlinear problem is the calculation of hydrostatic and undisturbed wave pressures over the instantaneous submerged part of the hull. These pressures are integrated over the submerged portion of hull surface and yield a combined hydrostatic and Froude Krylov force. In LAMP and many other time-domain seakeeping codes, these pressures are integrated over a 3-D panel model of the hull surface (Shin et al., 2003).

The hydrodynamic interaction between the ship and the wave also includes diffraction and radiation forces. These forces are also important for quantitatively correct numerical results, although they are usually smaller than the hydrostatic and Froude-Krylov forces. In potential-flow seakeeping simulation codes, these forces are typically computed via a potential-flow strip theory or panel method. LAMP has both body-linear (LAMP-2 and LAMP-3) and body-nonlinear (LAMP-4) panel methods available for diffraction and radiation forces (Shin et al., 2003). While the body-nonlinear formulation is essential for hydrostatic and Froude-Krylov forces, as they determine equilibria and topology of the phase space, the body-linear solutions for diffraction and radiation forces are acceptable for an engineering-level numerical modeling of capsizing in waves.

Even with the body-linear solution of the radiation and diffraction forces, the computational cost of simulations may be too expensive for a Monte-Carlo assessment of rare seakeeping phenomena such as capsizing. For an irregular seaway represented with a large number of wave components, just the integration of the body-nonlinear hydrostatic and Froude-Krylov pressure can be significant. To provide a faster simulation, an alternate calculation of the body-nonlinear hydrostatic and Froude-Krylov forces has been implemented, which is based on the instantaneous submerged volume, using Gauss' theorem to establish a relationship between the surface and volume integrals. The idea has been implemented into ROM simulation code "SimpleCode" (Weems and Wundrow, 2013; Weems and Belenky, 2023). Coupled with a coefficient-based approximation of diffraction and radiation forces, e.g. (Kim et al., 2023), this volume-based approach provides a computational speed close to the numerical solution of ordinary differential equations, while retaining the majority of the advantages of the body-nonlinear formulation.

The body-nonlinear formulation for hydrostatic and Froude-Krylov forces imposes a lower bound on the number of degrees of freedom for which a problem can be solved. As the pressure integration or volume calculation is based on the ship's motion relative to the wave surface, at least three degrees of freedom must be included: heave, roll and pitch. So considered, the body-nonlinear formulation for hydrostatic and Froude-Krylov forces takes care of stability variation in waves in a natural way.

3.2. Split-time method: formulation

The split-time method was originally developed for the estimation of a capsizing rate with time-domain simulation tools. It is based on the principles formulated by the study of the piecewise linear dynamical system, which was described in Section 2. If the principles formulated for a single degree-of-freedom dynamical system with piecewise linear restoring and described subsection 2.12 can be maintained, the approach can be extended to a dynamical system with 3 degrees of freedom. Consider a 3-DOF dynamical system describing the heave, roll and pitch motion of a ship in irregular waves travelling with some forward speed:

$$\boldsymbol{M_I}\dot{\vec{X}} = \vec{F}_{HSFK}\left(\vec{S},\zeta_W\right) + \vec{F}_{DR}\left(\vec{X},\dot{\vec{X}},\zeta_W\right) + \vec{F}_V\left(\vec{X}\right) + \vec{F}_G\left(\vec{S}\right) \tag{40}$$

where $\boldsymbol{M_I}$ is a matrix of inertia, $\vec{F}_{HSFK}$ is the vector valued-function of hydrostatic and Froude-Krylov forces, $\vec{F}_{DR}$ is the diffraction and radiation forces, ζ_W stands for the wave field, $\vec{F}_V$ is an approximation for viscous effect (including lifting forces from appendages), $\vec{F}_G$ is the gravity force, $\vec{X}$ is a vector of state variables and $\vec{S}$ is a vector of motion displacements. The two latter vectors are defined as:

$$\vec{X} = \vec{S} \cup \dot{\vec{S}}\ \vec{S} = (\zeta,\phi,\theta)^{\mathrm{T}} \tag{41}$$

where ζ,ϕ,θ are heave displacement, roll and pitch angles respectively, while superscript T stands for transposition. The heave displacement is defined in an Earth-fixed coordinate system. Roll and pitch are Euler angles following their traditional definition for ship and aircraft motion problems.

For the non-rare problem, LAMP, SimpleCode or an analogous seakeeping tool is applied to the dynamical system (40) with irregular wave forcing in order to produce a set of N_R ship motion records $\{\vec{X}_i\}_j; i = 1,..,N_j; j = 1,..,N_R$; each record contains N_j data points and represents the response to an independent realization of a stationary, stochastic model of ocean waves. Capsizing may or may not be present in this dataset. As capsizing is rare, the presence of capsizing would be rather exceptional. However, the absence or presence of capsizing should not be a problem for the application of the split-time method.

A special study was conducted to see the difference between rare solution with 3-DOF and 1-DOF (while heave and pitch were forced from unperturbed solution), but no qualitative difference in the results was observed.

3.3. Split-time method: critical roll rate

Based on the motion histories from a set of "non-rare" simulations, an intermediate level of roll ϕ_{m0} is selected that provides approximately 7–10 upcrossing over each 30 min of simulation time or 20–25 roll periods per a single crossing. This is an *ad hoc* number, i.e., based on experience. A study was conducted to see the influence the intermediate level, but no significant difference in the results was observed. For each upcrossing instant k, a series of short perturbation simulations are computed in order find the critical roll rate. The initial conditions for these short simulations are taken as:

$$\vec{X}_0 = (\zeta_{Uk},\phi_{m0},\theta_{Uk})^{\mathrm{T}} \cup (\dot{\zeta}_{Uk},\dot{\phi}_{Uk} + \Delta\dot{\phi},\dot{\theta}_{Uk})^{\mathrm{T}} \tag{42}$$

The index U indicates that a value was observed at the instant of upcrossing. $\dot{\phi}_{Uk}$ is the roll rate observed the instant of kth upcrossing of the intermediate level ϕ_{m0}. $\Delta\dot{\phi}$ is a perturbation of the roll rate at upcrossing. In order to make sure all the events during the transient are included in consideration, the duration of these short simulations needs to exceed the decorrelation time T_d estimated for the dataset. It is assumed that self-dependence does not extend beyond T_d. The roll rate perturbation $\Delta\dot{\phi}$ is systematically increased until capsizing has been observed, as illustrated in Fig. 9.

If the capsized equilibrium exists, capsizing is guaranteed for a sufficiently large value of the perturbed roll rate, as the invariant manifold around the capsized equilibrium (boundary of safe basin) does exist, see e.g., (Rainey et al., 1990). A value of the roll rate for a point at the invariant manifold also exists. Finding this point may not be always trivial as the boundary of the safe basin may be fractal. This creates

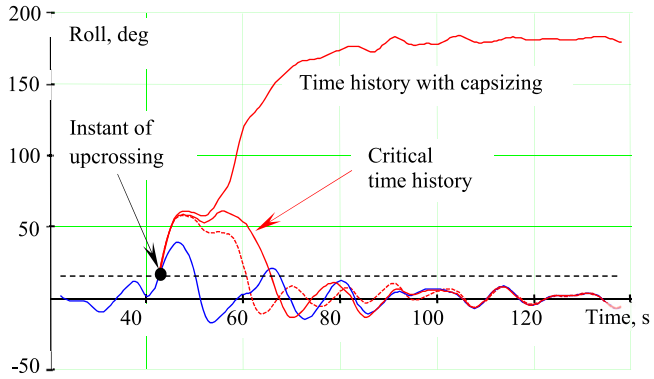

Fig. 9. Perturbed motion simulations (Belenky et al., 2018).

difficulties with the application of iterative algorithms, as they may not converge. As a result, perturbation has to be systematically increased until the capsizing is observed. The search for the perturbation of interest can contribute to the computational cost of the split-time method but is minimal relative to a Monte-Carlo evaluation.

Once capsizing has been observed, the simulation is repeated with slightly smaller perturbation $\Delta\dot{\phi}$ until capsizing is no longer observed, leading to the "critical time history" in Fig. 9. The value of perturbation corresponding to this critical time history is the critical perturbation $\Delta\dot{\phi}_{cr}$ with:

$$\dot{\phi}_{cr} = \dot{\phi}_{Uk} + \Delta\dot{\phi}_{cr} \tag{43}$$

The critical time history converges to the original (unperturbed) solution after about 60 s, which is close to a typical decorrelation time for roll motions. The convergence time T_{cnv} is determined by the difference between the perturbed and original solution computed for a specified number of consecutive roll cycles.

If a capsizing is present within this short simulation duration, a set of perturbed simulations are still run to determine the convergence time. If the originally observed capsizing occurs after this convergence time, it can be ignored, as it occurs beyond the influence of perturbations (Fig. 10a). The search for a critical roll rate continues, with the capsizing required to be within the convergence time. If the capsizing occurs within the convergence time, the value of the perturbed roll rate is set to satisfy $\dot{\phi}_{Uk} + \Delta\dot{\phi}_{cr} = 0$. If capsizing disappears, the search for the critical roll rate continues as described above. If capsizing remains for an initial roll rate of zero, the critical roll rate is set to zero as well: $\dot{\phi}_{cr} = 0$. This case is indicated in Fig. 10b.

The results of calculation of critical roll rate for a single record are illustrated in Fig. 11. This record has been taken from Weems et al. (2023), and it is for the ONR Topsides Series tumblehome configuration (Bishop et al., 2005), sailing in stern-quartering waves (heading 45°) with a constant forward speed of 6 knots in irregular waves with significant wave height of 9 m and a modal period of 14 s. The seaway is modeled using a Bretschneider (1959) spectrum and corresponds to a high sea state 7 or low sea state 8. The value of GM was 2.2 m. 3-DOF (Heave-Roll-Pitch) simulations were carried out with volume-based tool SimpleCode (Weems and Belenky, 2023) with nominal coefficients for added mass and damping and without diffraction.

The record in Fig. 11a contains an episode of large rolling at around 1000 s, a close-up of which is shown in Fig. 11b. The intermediate roll

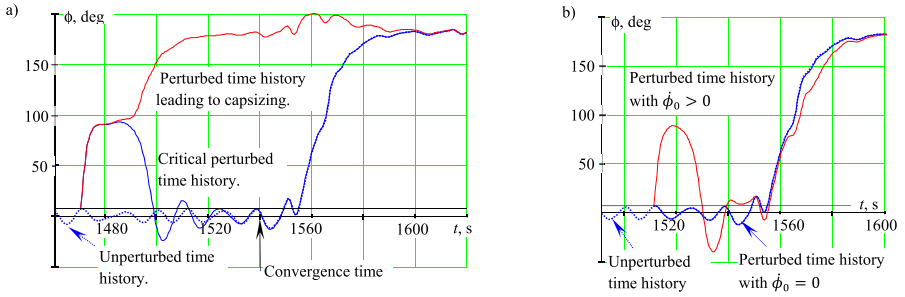

Fig. 10. Processing observed capsizing event (a) capsizing occurs after convergence time; (b) capsizing occurred during the convergence time.

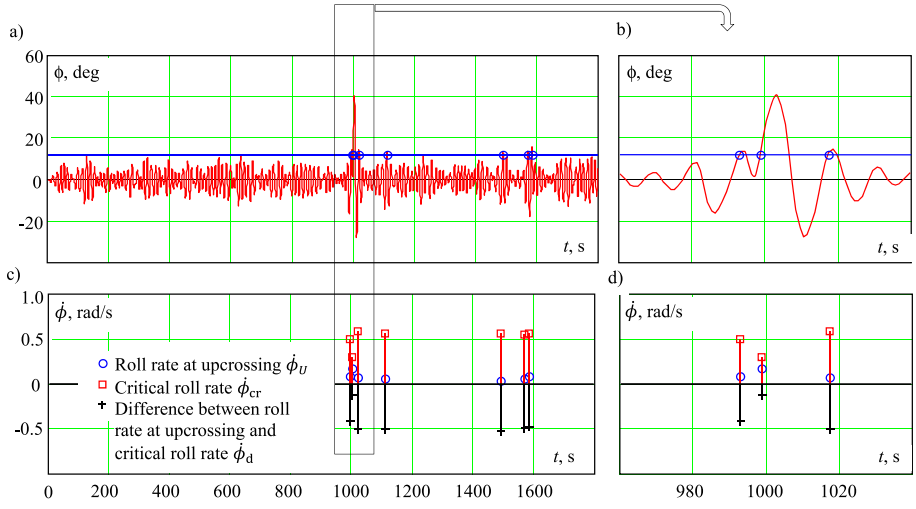

Fig. 11. Visualization of the results of calculation of critical roll rate for a single record: (a) roll time history (b) close-up of roll time history (c) critical roll rate and associated values, (d) close-up of critical roll rate and associated values.

level was set to 12° leading to a total of seven upcrossings, identified by circles in Fig. 11a and b. Fig. 11c shows the values of roll rate $\dot{\phi}_1$ at the instants of these upcrossings (also shown with circles), while boxes identify the values of the critical roll rates $\dot{\phi}_{cr}$. The difference between the roll rate at upcrossing and the critical roll rate $\dot{\phi}_d$ are indicated with crosses. Fig. 11d contains a close-up of the large roll angle episode around 1000 s.

Note that the upcrossing prior to the large roll angle yields the smallest value of the critical roll rate, $\dot{\phi}_{cr} = 0.29$ rad/s, while the rest of the values of the critical roll rate are around 0.5 rad/s. The roll rate at this upcrossing is $\dot{\phi}_1 = 0.165$ rad/s, while the other observed values are around 0.03–0.08 rad/s. The rate difference $\dot{\phi}_d$ = -0.125 rad/s is the largest (least negative) among the observed values of $\dot{\phi}_d$, which are otherwise in the range of −0.5 to −0.4 rad/s. Since a zero-value of $\dot{\phi}_d$ is associated with capsizing, the closest value of $\dot{\phi}_d$ to zero would be expected to produce the largest roll angle, so this seems reasonable. Small value of the critical roll rate is consistent with pure loss of stability.

Fig. 12 provides some insight into the pure loss of stability associated with the large roll event, which was evident in the smaller value of critical roll rate for the associated upcrossing. Fig. 12a shows three instantaneous GZ curves, while Fig. 12b identifies the time instances when these GZ curves were computed. The red GZ curve computed early in the roll event at $t = 997.5$ s has no positive stability, while the other two GZ curves show some recovery of stability as the wave passes.

These stability-in-waves evolutions show how the large roll angle of 40° observed at $t = 1002.5$ s is induced by a loss of stability a short time earlier. Fig. 12a also shows the calm-water GZ curve. It is interesting to note that the calm-water GZ curve does not indicate any reason for intact stability concerns: GZ maximum is around 0.75 m, occurring around 46° while the range of stability is above 90°. Nevertheless, a deterioration of the stability in waves lead to a 40° roll angle. A similar type of analysis can be found in more detail by Spyrou et al. (2014). The algorithm for evaluating the instantaneous GZ curves in waves is described in Belenky and Weems (2008a).

This example illustrates an important capability of the present approach – the critical roll rate contains information on "things that have not yet come to pass," i.e., possible scenarios of capsizing with account of future variation of stability in waves.

The perturbed simulations provide important information about potential capsizing. The simulation time is "split" between the main and perturbed simulation, which was the inspiration to name the method "split-time". Another name used in the literature is "motion perturbation method" (MPM), which reflects the key role that perturbation plays in the approach.

3.4. Hydrodynamic memory

A significant challenge of using motion perturbation methods with numerical seakeeping simulation tools is the consideration of the hydrodynamic memory. Hydrodynamic memory is an effect in which the flow field and forces of the wave-body hydrodynamic interaction problem are dependent on the short- to medium-term history of the solution and cannot be completely quantified as functions of the instantaneous state variables and their derivatives, as can be done for a model based on ordinary differential equations (ODEs). In potential flow seakeeping models, this memory is associated with the unsteady disturbance wave field generated by the ship's unsteady motion (radiation waves), interaction with the incident wave (diffraction waves) and forward speed (Kelvin waves). In viscous flow solvers (e.g. URANS and LES), they will also be associated with the generation and evolution of vortical flow structures and the like.

Motion perturbation analysis requires simulations starting at crossing points of the non-rare simulations with variations to selected state variables, which will be the roll velocity for the present capsizing problem. To save the complete state of the calculation is relatively straight forward, including the unsteady free surface disturbance, and then the perturbation simulation from this point is restarted. However, large variations in the roll rate generally result in a significant transient behavior due to the impulsive change in velocity, which often lead to instability in the free surface potential flow solution.

The simplest solution to the problem is to use an ODE-like approximation for the disturbance wave forces in the perturbation simulations rather than attempting to solve the free-surface potential flow problem. In its most basic form, this consists of the prescribed added mass and damping coefficients. LAMP has an option to turn off the disturbance wave forces and use added mass and damping coefficients instead (the option is usually referred as LAMP-0 model). This option was used in the implementation and initial testing of the MPM described above. Validation cases described in Weems et al. (2023) utilized the similar approach, but implemented in the volume-based tool (Weems and Belenky, 2023).

As these provide an explicit calculation of the radiation and diffraction effects in terms of the state variables, they have no problem with the perturbation to the roll rate or other state variables and have the significant advantage that they result in a relatively fast calculation of the perturbation simulations. The approach is, however, approximate and the effect of the approximation will need to be quantified.

The incorporation of the conventional time-domain free surface potential flow solution in the perturbation simulations corresponds to introducing the perturbation of the motion while maintaining the stability and correctness of the flow solution. To avoid instability and minimize transient effects, the perturbation begins 10–20 s before the crossing event, with prescribed motions during the period up to the

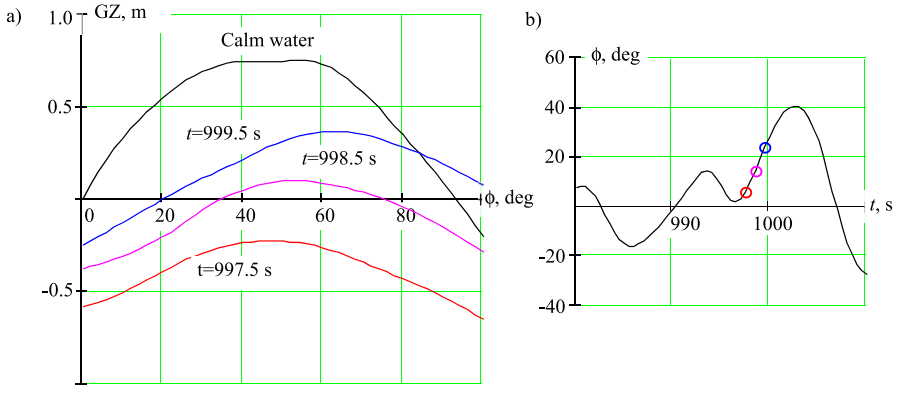

Fig. 12. Pure loss of stability (a) GZ curves in waves (b) Time history of roll: color circles correspond to the time instances where respective GZ curves were computed.

event. The prescribed motions are based on the motions from the non-rare simulation with the velocity perturbation feathered in over this time. An advantage of such an approach is that it can be implemented with regular check-pointing of the non-rare solution without having to identify and save crossing points during the non-rare simulations. A disadvantage of such an approach is that it is relatively computationally expensive compared to only identifying upcrossings.

An example of these calculations is shown in Fig. 13, where LAMP-2 was used for perturbed simulation, where diffraction and radiation were computed with a Rankine-source scheme over the mean wetted surface. The unperturbed solution is shown in dashed black line, the perturbed solution being just short of capsizing is depicted as solid blue line, while capsizing time history is given in red. The configuration was ONR Topside Series tumblehome hull, for which the 3D model and characteristics are shown in Fig. 14. The heading was 45 deg. (stern quartering seas) with forward speed of 6 knots in a sea state with significant wave height of 9 m and modal period of 14 s. The value of GM was 2 m.

Another approach toward incorporating memory into the perturbation simulations would be to use an impulse response function (IRF) solution of the disturbance potential. The IRF-based formulation of the wave-body interaction problem uses body-linear solutions of the impulsive radiation and diffraction problems that are convoluted with the wave and motion time history to provide a very rapid approximate body-nonlinear solution. The method has long been applied for constant course and speed seakeeping simulations (Weems et al., 2000), and was adapted to the perturbation simulations in which the ship can be assumed to have constant course and speed for the duration of the perturbation. The computational stability issues were considerably mitigated, while numerical results were very similar to in Fig. 13.

3.5. Calculation of critical roll rate for 6-DOF

The split-time method can also be applied to 6-DOF simulations. An example, computed with LAMP-0, is shown in Fig. 15. The unperturbed solution is shown in dashed black line, the perturbed solution being just short of capsizing is depicted as solid blue line, while capsizing time history is given in red. The ship is again the ONR Topsides tumblehome hull and the wave conditions are the same as the shown in Fig. 14. The hull sway force and yaw moment were approximated with hull lifting coefficients based on experimental data of a similar hull. Rudder course control was implemented with a proportional gain of 2 and differential gain 0.5.

The main difference of 6-DOF vs. 3-DOF calculations is apparent in Fig. 15 as a lack of convergence. In the absence of capsizing, the perturbed solution does not necessarily converge to the unperturbed solution. The reason can be understood from Fig. 15c and f, showing a trajectory in the horizontal plane and a time history of the surge velocity. As the horizontal plane motions (surge, sway and yaw) are

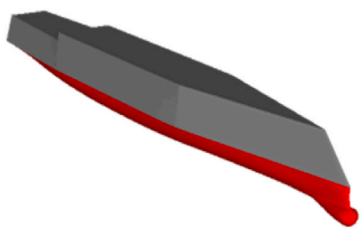

Length: 154 m
Breadth: 18.8 m
Draft: 5.5 m
GM: 2 m
Forward speed: 6 kn
Heading: 45 deg
Significant wave height: 9 m
Spectral modal period: 14 s

Fig. 14. ONR Topside Series tumblehome configuration for LAMP simulations.

included, the perturbation moves the ship away from the original path. The surging velocity is also different, so the perturbed solution ends up in a different place in the wave field, resulting in a phase shift of the waves as encountered by the ship.

The time of convergence was used to determine if the capsizing observed in the perturbed solution could be attributed to that perturbation. This is essentially a problem of self-dependence – how long a current value of a stochastic process is influenced by its values in the past. A decorrelation time can also be used as an approximate metric of self-dependence. The decorrelation time is defined as an interval where the autocorrelation is no longer significant. The autocorrelation function is a normalized autocovariance function. The latter is estimated as:

$$\widehat{R}_k = \sum_{j=1}^{N_R} \frac{W_j}{N_j} \sum_{i=1}^{N_j-k} \left(\{\phi_i\}_j - \widehat{E}_\phi\right)\left(\{\phi_{i+k}\}_j - \widehat{E}_\phi\right); \tag{44}$$

$$k = 0, 1, \ldots N_k$$

where $\{\phi_i\}_j; i = 1, .., N_j;\ j = 1, .., N_R$ is a roll motion dataset consisted of N_R records, each of which contains N_j points. The "hat" above a symbol means that it is "an estimate from the data" rather than a theoretical value. $\widehat{E}_\phi$ is mean value of roll angles estimated over the entire dataset:

$$\widehat{E}_\phi = \sum_{j=1}^{N_R} \frac{W_j}{N_j} \sum_{i=1}^{N_j} \{\phi_i\}_j \tag{45}$$

where W_j is a statistical weight of each record defined as:

$$W_j = N_j \cdot \left(\sum_{j=1}^{N_R} N_j\right)^{-1} \tag{46}$$

where N_k is the number of time increments for which autocorrelation function can be reasonably estimated.

Time lag is an argument of the autocorrelation function. The estimate of the autocorrelation function for larger time lag is less accurate as fewer data points are available for larger time lags. This problem is partially solved by penalizing the contribution to $\widehat{R}_k$ from the larger lags with $(N_j - k)/N_j$. In principle, N_k can be set equal to max(N_j), but the

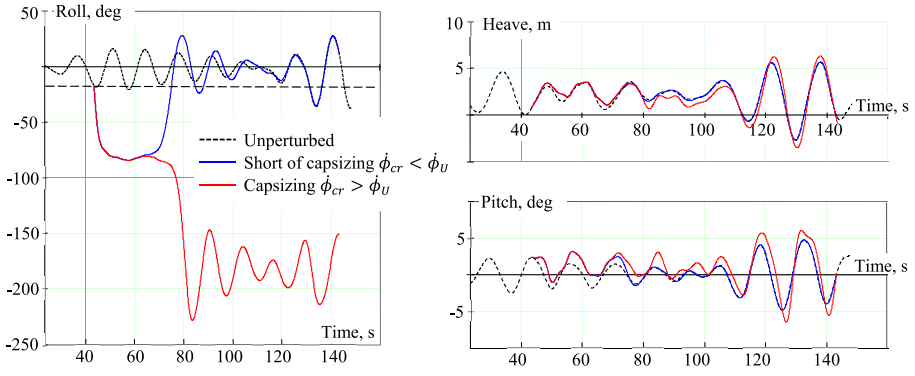

Fig. 13. Perturbation calculations with LAMP-2, with diffraction and radiation computed during simulations with Rankine-source method (Weems and Belenky, 2017).

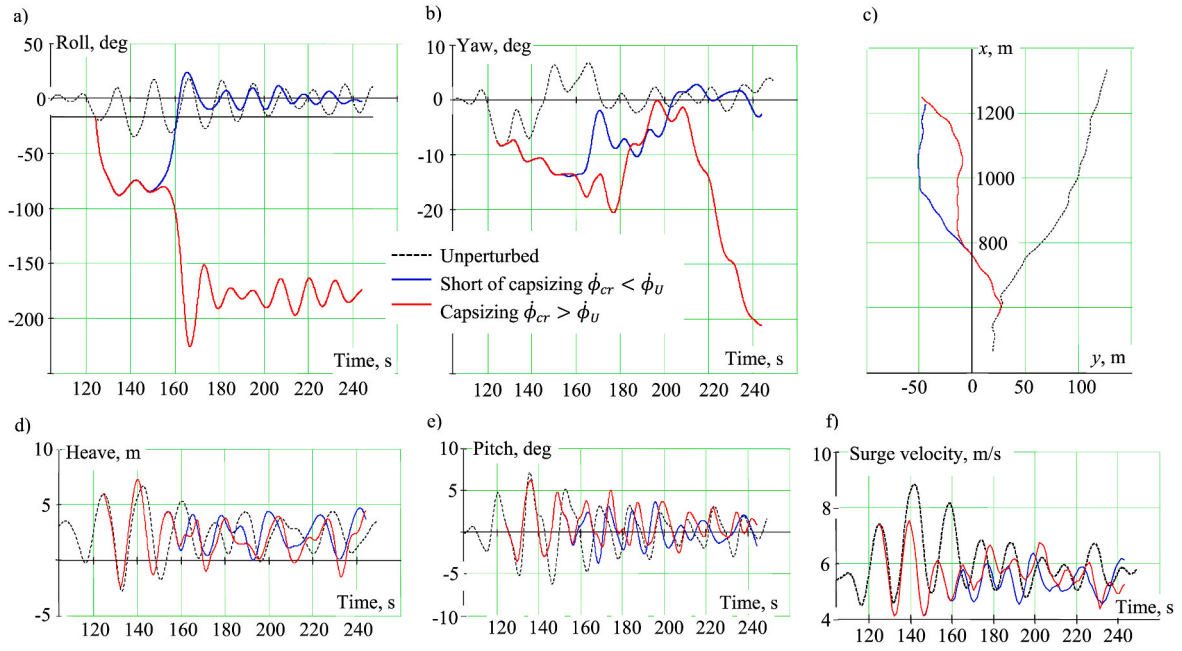

Fig. 15. Perturbation calculations with 6-DOF LAMP-0: (a) Roll time history (b) Yaw time history (c) Trajectory (d) Heave time history (e) Pitch time history (f) Time history of surge velocity.

calculation of decorrelation time usually requires fewer points. The estimate (44) is biased, but the bias is small for realistic values of N_j. The estimate can be de-biased with $N_j/(N_j-1)$. Finally, the autocorrelation function is computed by the normalization of autocovariance function with its first term (which is the variance):

$$\hat{r}_k = \frac{\hat{R}_k}{\hat{R}_0} \tag{47}$$

Fig. 16 illustrates a scheme for estimating the decorrelation time. The significance level needs to be selected, and its value is usually taken as 0.05 or 0.01. An envelope of the autocorrelation function is computed as a line connecting the absolute values of its peaks. The decorrelation time is where the envelope of the autocorrelation crosses the significance level for the first time.

This decorrelation time is employed instead of the convergence time. In all other regards, the calculation of the critical roll rate for a 6-DOF perturbation is identical to that for a 3-DOF case. A study was conducted to see the difference if decorrelation time is applied in the 3-DOF case instead of convergence time, but no significant difference in the results was observed.

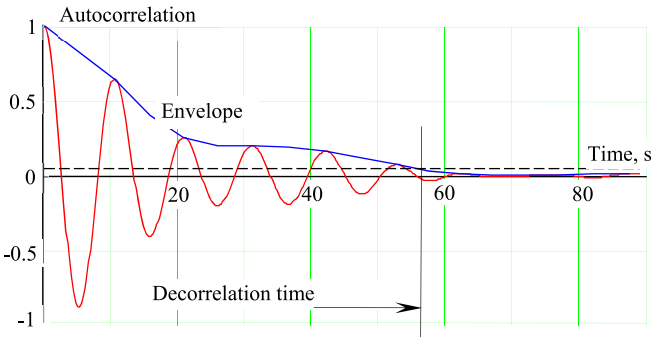

Fig. 16. Calculation of decorrelation time for roll motions.

4. Tail of the distribution of capsizing metric

4.1. Capsizing metric and its extrapolation

The algorithm for calculation of the critical roll rate, described in the Section 3.2, allows the evaluation of the likelihood of events, not observed in the data. The physics associated with the transition to the capsized equilibrium, including the effects of large roll angle such as water-on-deck and bilge keel emergence, can be included in the perturbation simulations. Therefore, these contributing physics from large roll are reflected in the critical roll rate.

To complete the calculation, a distribution of the differences between the roll rate at upcrossing and the critical roll rate needs to be modeled from the values computed for each upcrossing. However, the entire distribution is not necessary for estimating the probability of capsizing; as capsizing in realistic conditions is rare. It is sufficient to model only the tail of the distribution. The numerical approach based on the critical roll rate essentially transforms the capsizing probability problem into an ordinary extrapolation problem, as illustrated in Fig. 17. This extrapolation problem is legitimate as the information on the proximity of capsizing is present in the data.

4.2. Application of extreme value theory

As was mentioned in Section 1.3 of the Introduction, the mathematical background for the distribution tail fitting is based on the extreme value theory, see e.g., (Coles, 2001). The largest value in a sample of independent data points asymptotically follows a Generalized Extreme Value (GEV) distribution, irrespectively of the distribution of

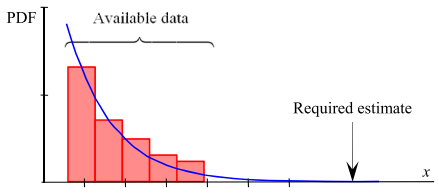

Fig. 17. The problem of statistical extrapolation.

all of the data points. Extreme value theory is used in many applications and has recently been included in the framework of the IMO Second Generation Intact Stability Criteria, as described in Section 5.3.1 of Appendix 4 to the Explanatory Notes to the Interim Guidelines on the Second Generation Intact Stability Criteria, MSC.1/Circ. 1652 (IMO, 2023).

To illustrate this principle, consider an example from the cited Explanatory Notes. In general, the largest value from a sample of n independent data points is distributed as:

$$\mathrm{PDF}_1(x|n) = \mathrm{PDF}(x)(\mathrm{CDF}(x))^{n-1} \tag{48}$$

where $\mathrm{PDF}(x)$ and $\mathrm{CDF}(x)$ are the probability density and cumulative distribution functions of the sampled random variable x respectively. This distribution is usually referred as the "underlying distribution" and is assumed to be normal for this example. Equation (48) is correct for any underlying distribution, as soon as the sample points are independent. The Fisher-Tippet-Gnedenko (or the first extreme value) theorem states that with the increase of n, the distribution (48) trends towards the GEV distribution:

$$\mathrm{PDF}_{GEV}(x) = \begin{cases} \exp(-y)\cdot\exp(-\exp(-y)) \\ \text{for } \xi = 0 \\ (1+\xi\cdot y)^{-(1+1/\xi)}\exp\left(-(1+\xi\cdot y)^{-(1/\xi)}\right) \\ \text{for } \xi \neq 0 \cap \xi\cdot y > -1 \\ 0 \quad \text{otherwise} \\ \text{where} \quad y = \dfrac{x-\mu}{\sigma} \end{cases} \tag{49}$$

where ξ is a shape parameter, σ is a scale parameter and μ is a location parameter. The convergence of the distribution of the largest value among the sample of n-points is shown in Fig. 18 (underlying distribution is standard normal).

When the GEV distribution is used to extrapolate outside of the observed data, the parameters are estimated from the available sample, allowing an evaluation of the probability outside of the observed data, as shown in Fig. 17. The data points used for the estimation are essentially the largest values in a sample, so only a single point from a sample can be used. To increase data utilization, a "block maxima" approach can be used – the sample is subdivided into "blocks", large enough so its maxima can be considered independent. Independence of data is one of the requirements for using GEV.

Another way to improve data utilization is fitting a tail of the distribution, using only the data points above some large-enough threshold. The tail is expressed by the conditional GEV over the exceedance of a threshold w, the result is known as Generalized Pareto Distribution (GPD):

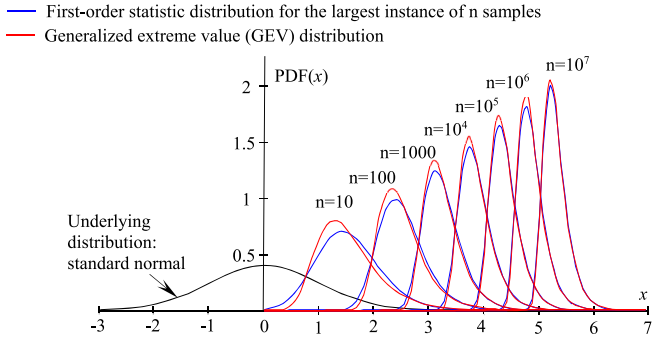

Fig. 18. Convergence of the distribution of the largest value in a sample to a GEV with an increasing number of samples (MSC.1/Circ. 1652).

$$\mathrm{pdf}_{GPD}(x) = \begin{cases} \dfrac{1}{\sigma}\exp\left(-\dfrac{x-w}{\sigma}\right) \text{ for } \xi = 0 \\ \dfrac{1}{\sigma}\left(1+\xi\dfrac{x-w}{\sigma}\right)^{-(1+1/\xi)} \text{ for } \xi \neq 0 \text{ and } \xi\dfrac{x-w}{\sigma} > -1 \\ 0 \quad \text{otherwise} \end{cases} \tag{50}$$

The shape parameter ξ and the scale parameter σ are the same as in equation (49).

Equation (50) represents the essence of the Pickands-Balkema-de Haan (or the second extreme value) theorem, stating that a distribution above the large-enough threshold can be approximated with GPD. Note that the GPD threshold w has a completely different meaning than that of the roll-angle intermediate level ϕ_0 (to avoid confusion, the term "threshold" is used in this paper only for distribution tail definition, while the term "level" is applied for the boundary between the non-rare and rare problems).

The scale parameter σ must be positive (as the PDF cannot be negative), while the shape parameter ξ can be either positive or negative. For the case $\xi = 0$, the GPD becomes an exponential distribution for the variable x-w with the parameter $1/\sigma$. A negative shape parameter imposes a limitation on the variable x:

$$w < x < w - \sigma/\xi\,; \quad \xi < 0 \tag{51}$$

This limitation formally introduces a right bound for the negative values of shape parameter, located at $x = w - \sigma/\xi$. The shape parameter therefore defines the type of tail: heavy, exponential or light, as shown in Fig. 19.

GPD can also be used for extrapolation as well as GEV. This could be seen as being more efficient from the data utilization standpoint; however, it requires the determination of a threshold that is "large enough". The choice between GEV and GPD for extrapolation is a matter of preference. The authors have used GPD for the study of the distribution tail of capsizing metric.

4.3. Metric definition and declustering procedure

It is convenient to define a formal metric of the likelihood of capsizing, computed at the kth upcrossing of a level ϕ_0 as:

$$h_k = c_m + \dot{\phi}_{Uk} - \dot{\phi}_{cr};\ c_m = 1\ rad/s \tag{52}$$

The constant c_m is introduced for convenience only. The difference $\dot{\phi}_{Uk} - \dot{\phi}_{cr}$ is negative, as capsizing is not expected to be observed during the simulations. If the difference $\dot{\phi}_{Uk} - \dot{\phi}_{cr}$ is used as the metric, capsizing is expected when $\dot{\phi}_{Uk} - \dot{\phi}_{cr} = 0$, so the target for extrapolation would be zero. The constant c_m simply shifts the extrapolation target to the right, placing the distribution of the metric into the positive semi-axes. The choice for the numerical value for c_m is an arbitrary large value for roll rate to ensure that the domain of the metric is positive (for convenience and expressive graphics).

The values of a capsizing likelihood metric are computed at each upcrossing. Thus, the metric values are not necessarily independent random variables as the upcrossing instants can be grouped or clustered due to self-dependence of the roll motion process. At the same time,

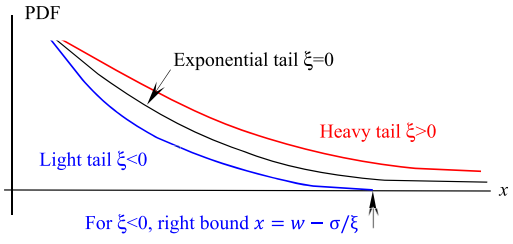

Fig. 19. Types of tails.

extreme value theory is formulated for independent random variables only, so any self-dependence has to be removed from the computed set of metric values. The procedure of the self-dependence removal can be referred to as "declustering".

Declustering is illustrated in Fig. 20. First, the clusters are identified with the time of influence for an individual crossing. The convergence time (Fig. 10) can be used for 3-DOF rare problem formulation. The decorrelation time (Fig. 16) is applicable for both 6-DOF and 3-DOF rare problem formulations. As can be seen from Fig. 20, the upcrossing data are included in a cluster until there is no more data available within the influence time. Declustering is completed by selecting the largest value of the metric observed within each cluster.

The necessity for declustering provides guidance on the selection of the intermediate level ϕ_{m0}. If the level was chosen too low, clusters will be long, resulting in low computational efficiency, as many of the metric values will not be selected, while each of them carries a certain computational cost. If the intermediate level is selected too high, there will be fewer crossing and the simulation dataset has to be longer, which also carries a certain computational cost.

4.4. Approximation of tail of distribution of capsizing metric with GPD

For the approximation of the tail of the distribution of capsizing metric with GPD, its shape and scale parameters must be estimated as well as a value of the threshold needs to be found. The threshold should be "large enough" to claim extreme value properties, i.e. the tail of observed distribution behaves similar to GPD. For the "large enough" threshold, the shape parameter should no longer depend on the threshold value, see e.g., (Coles, 2001). To find the value of this "large enough" threshold, a number of candidate thresholds are considered, so shape and scale parameters need to be estimated for these thresholds.

The maximum likelihood estimator (MLE) method is a standard way of estimating the parameters for the GPD distribution. The idea of MLE is that sample data points have the largest probability under GPD parameters close to the true parameters, because they were observed. Thus, the best estimates for the parameters should maximize a likelihood function defined as a joint probability of the sample points. To minimize the negative logarithm of the likelihood function is more convenient:

$$L(\xi,\sigma)=N\cdot\ln(\sigma)+\left(1+\frac{1}{\xi}\right)\sum_{i=1}^{N}\left(1+\xi\frac{z_i}{\sigma}\right) \tag{53}$$

where N is the number of data points above a threshold w and $z_i=h_i-w$ are the sample data points above a candidate threshold w.

The two-dimensional log-likelihood (53) can be rewritten as a function of only one argument (Grimshaw, 1991):

$$L(k_s)=N\cdot ln\left(N\cdot\left(\sum_{i=1}^{N}\left(1+\frac{1}{k_s z_i}\right)\right)^{-1}-1\right)-N\cdot ln(k_s) \tag{54}$$
$$+N\cdot ln\left(N-\sum_{i=1}^{N}\left(1+\frac{1}{k_s z_i}\right)\right)^{-1}\sum_{i=1}^{N}(1+k_s z_i)$$

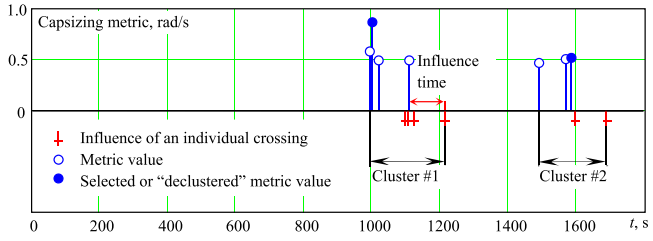

Fig. 20. Declustering of the metric of capsizing likelihood.

where $k_s=\xi/\sigma$.

In principle, it is possible to differentiate the function (54) and solve an algebraic equation for the zero-value of k_s. The function (54), however, has a relatively shallow minimum at the candidate thresholds of interest, as illustrated in Fig. 21. The authors have had better success using minimization routines, available from a standard numerical library. Minimization algorithms usually requires an initial value that can be obtained through the estimates of the mean $\widehat{E}_z$ and variance $\widehat{V}_z$ of the data above the candidate threshold:

$$\widehat{\xi}_0=0.5\left(1-\frac{\widehat{E}_z^2}{\widehat{V}_z}\right),\quad \widehat{\sigma}_0=0.5\widehat{E}_z\left(1+\frac{\widehat{E}_z^2}{\widehat{V}_z}\right) \tag{55}$$

Once $\widehat{k}_s=\mathrm{argmin}(L(k_s))$ is found, the estimates of the shape and scale parameters are:

$$\widehat{\xi}=N\cdot\left(\sum_{i=1}^{N}\left(1+\frac{1}{\widehat{k}_s z_i}\right)\right)^{-1}-1,\qquad \widehat{\sigma}=\frac{\widehat{k}_s}{\widehat{\xi}} \tag{56}$$

The distribution of the estimates of the shape and scale parameters can be taken as bivariate normal (Smith, 1987). To define it, mean values, variances, and correlation coefficient must be found. The MLE method is known to lead to an unbiased estimate, so the mean values of the parameters are simply equal to the estimates themselves. The minimization of (54), and the calculation with (56) produce estimates for the mean values of the shape and scale parameters. Their variances and the correlation can be estimated using the delta-method, i.e., expanding (54) with Taylor series and then interpreting that expansion as a deterministic function of random variables, see Boos and Stefanski (2013). As a result, the covariance matrix is expressed through the second-order derivatives of the log-likelihood function (53):

$$\widehat{\mathrm{Cov}}(\xi,\sigma)=\begin{pmatrix}\partial^2L/\partial\xi^2 & \partial^2L/\partial\xi\partial\sigma\\ \partial^2L/\partial\xi\partial\sigma & \partial^2L/\partial\sigma^2\end{pmatrix}^{-1}=\begin{pmatrix}\widehat{V}_\xi & \widehat{r}_{\xi\sigma}\left(\widehat{V}_\xi\widehat{V}_\sigma\right)^{0.5}\\ \widehat{r}_{\xi\sigma}\left(\widehat{V}_\xi\widehat{V}_\sigma\right)^{0.5} & \widehat{V}_\sigma\end{pmatrix} \tag{57}$$

where

$$\frac{\partial^2L}{\partial\xi^2}=\frac{2}{\xi^3}\sum_{i=1}^{N}\ln\left(1+\xi\frac{z_i}{\sigma}\right)-\frac{2}{\xi^2}\sum_{i=1}^{N}\frac{z_i}{\sigma+\xi z_i}-\left(1+\frac{1}{\xi}\right)\sum_{i=1}^{N}\left(\frac{z_i}{\sigma+\xi z_i}\right)^2$$
$$\frac{\partial^2L}{\partial\sigma^2}=\frac{N}{\xi\sigma^2}-\left(1+\frac{1}{\xi}\right)\sum_{i=1}^{N}\frac{1}{(\sigma+\xi z_i)^2}$$
$$\frac{\partial^2L}{\partial\xi\partial\sigma}=\frac{N}{\xi^2\sigma}-\frac{1}{\xi^2}\sum_{i=1}^{N}\frac{1}{\sigma+\xi z_i}-\left(1+\frac{1}{\xi}\right)\sum_{i=1}^{N}\frac{z_i}{(\sigma+\xi z_i)^2} \tag{58}$$

Equations (57) and (58) allow the construction of a confidence interval for the estimates of the parameters:

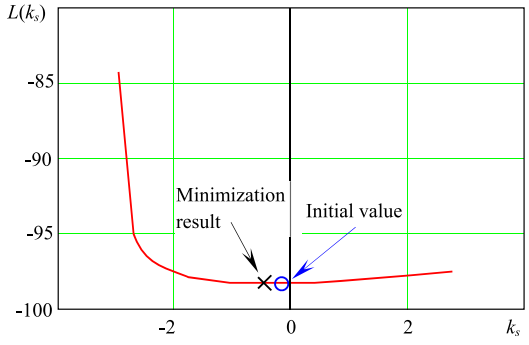

Fig. 21. Negative log likelihood for the threshold value $w=0.546$ rad/s.

$$\widehat{\xi}_{up,low} = \widehat{\xi} \pm Q_N \widehat{V}_{\xi}^{0.5}, \quad \widehat{\sigma}_{up,low} = \widehat{\sigma} \pm Q_N \widehat{V}_{\sigma}^{0.5} \tag{59}$$

where Q_N is standard normal quantile. For a confidence probability, $P_\beta = 0.95$ and $Q_N = 1.96$.

As mentioned above, to find what value of the threshold support the claim of extreme-value properties, GPD-like behavior must be observed in the data. The shape parameter not depending on the threshold is one of the indicators of this GPD-like behavior. As the estimate of the shape parameter is a random number, checking if it is constant should be interpreted in a statistical sense, i.e. plotting a line though its confidence interval, see Fig. 22.

The scale parameter is not required to be constant and cannot be used directly. Instead, the modified scale parameter is defined as:

$$\sigma_m = \sigma - \xi w \tag{60}$$

Similar to the shape and scale parameter, the mean value of its estimate is equal to itself, while the variance can be computed from the covariance $\mathrm{Cov}(\xi, \sigma)$:

$$\widehat{V}_{\sigma_m} = \vec{W}^T \widehat{\mathrm{Cov}}(\xi, \sigma) \vec{W}, \qquad \vec{W} = \begin{pmatrix} -w \\ 1 \end{pmatrix} \tag{61}$$

The modified scale parameter is expected to be a constant when the GPD is applicable, so the same rules for the choice of the threshold can be used, as illustrated in Fig. 23. The selection of the threshold is the same as in Fig. 22, but this is a coincidence and may not be the case for other data sets.

The idea to search the threshold that gives the "best" fit in terms of accuracy was implemented in the *ad hoc* method described by Reiss and Thomas (2007), where it was referred to as a possibility for an automatic procedure. A similar (but not exactly the same) approach has been employed here, making use of the already estimated shape parameters. The threshold is searched by minimizing the following function:

$$f(w_k) = \frac{1}{N_{tr} - k} \sum_{i=k}^{N_{tr}-1} (N_{tr} - i)^b \times \left| \widehat{\xi}_i - \mathrm{md}\left(\widehat{\xi}_k, \ldots, \widehat{\xi}_{N_{tr}}\right) \right| \tag{62}$$

where N_{tr} is a number of candidate thresholds considered, md() is a median function, and $\widehat{\xi}_k, \ldots, \widehat{\xi}_{N_{tr}}$ are estimates of shape parameter above the k-th threshold. A value of 0.5 was taken for b. A plot of (62) is shown in Fig. 24. The selected threshold is noticeably larger, compared to the selections from the shape parameter plot in Fig. 22 and the modified scale parameter plot in Fig. 23. Interestingly, the function (62) experiences a local minimum where the previous selections for the threshold was made.

Following recommendations in Reiss and Thomas (2007), the squared difference from the mean was considered instead of the absolute value of the difference from the median:

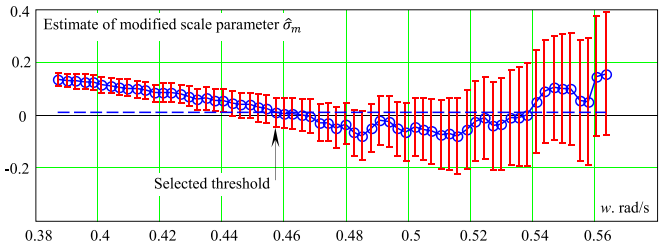

Fig. 23. Modified scale parameter plot.

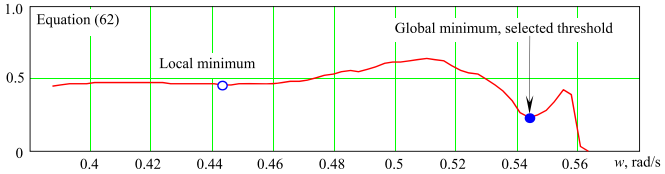

Fig. 24. Appearance and minima of equation (62).

$$f(w_k) = \frac{1}{N_{tr} - k} \sum_{i=k}^{N_{tr}-1} (N_{tr} - i)^b \times \left(\widehat{\xi}_i - \mathbb{E}\left(\widehat{\xi}_k, \ldots, \widehat{\xi}_{N_{tr}}\right) \right)^2 \tag{63}$$

where $\mathbb{E}$ is an averaging operator. Function (63) is plotted in Fig. 25 and its interpretation seems to be similar to Fig. 24. The selected threshold is also similar.

Mager (2015) developed methods for automatic threshold selection using the minimum of prediction error as a criterion. This approach was successfully applied for exponential distribution (see subsection 4.7). However, the application of the prediction error criterion for GPD remains for future research.

The highest threshold among those identified by the four applied methods is the final selection. The justification of selecting the highest

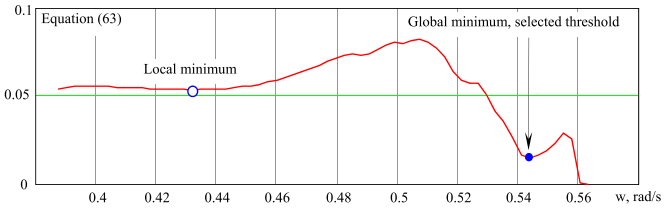

Fig. 25. Appearance and minima of equation (63).

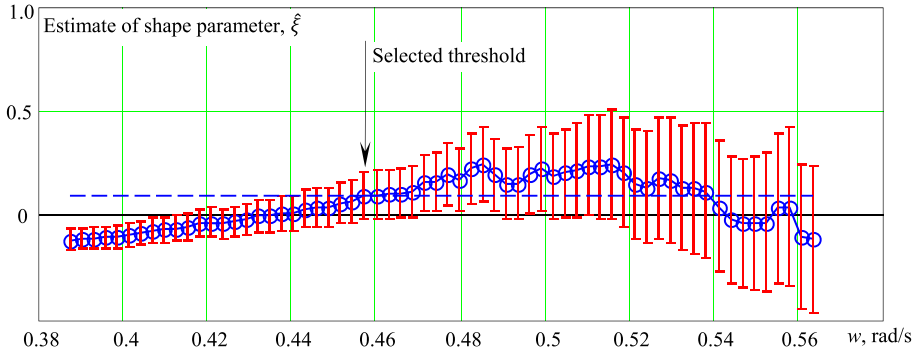

Fig. 22. Shape parameter plot.

threshold is that a threshold is identified based on the applicability of the extreme-values properties, so these properties also can be claimed for all of the thresholds above the selected. The highest threshold value is supported by all four considered methods.

4.5. GPD-extrapolated estimate and its uncertainty quantification

Once the GPD parameters (including the threshold) have been evaluated, the estimate of the conditional probability of capsizing (under the condition that the roll angle crosses the intermediate level and the value of metric exceeds the chosen threshold w) can be expressed as:

$$\widehat{P}(\dot{\phi}_1 > \dot{\phi}_{cr} | h > w) = \widehat{P}(h > c_m | h > w) = \begin{cases} \left(1 + \widehat{\xi}\frac{c_m - w}{\widehat{\sigma}}\right)^{-1/\widehat{\xi}} \text{ for } \widehat{\xi} > -\dfrac{\widehat{\sigma}}{c_m - w} \\ 0 \text{ for } \widehat{\xi} \le -\dfrac{\widehat{\sigma}}{c_m - w} \end{cases} \tag{64}$$

where $c_m = 1\ rad/s$, see equation (52).

Formula (64) describes an estimate, which is a random variable, so its uncertainty must be addressed. It can be considered a deterministic function g of random arguments, which are the estimates of the shape and scale parameters:

$$\widehat{P}(h > c_m | h > w) = g(\widehat{\xi}, \widehat{\sigma}) \tag{65}$$

The appearance of the function $g(\widehat{\xi}, \widehat{\sigma})$ is shown in Fig. 26 (Belenky et al., 2014).

The function $g(\widehat{\xi}, \widehat{\sigma})$ has the following property, which will be used below. Take $c_m - w = 1$ for notational simplicity. Consider any line segment $s = \{g(\widehat{\xi}, \widehat{\sigma}) : \widehat{\xi} = a + b\widehat{\sigma}, \widehat{\sigma} \in [\sigma_1, \sigma_2]\}$ falling inside the range of possible parameter values $\{(\widehat{\xi}, \widehat{\sigma}) : \widehat{\sigma} > 0, \widehat{\xi} > -\widehat{\sigma}\}$ where $g(\widehat{\xi}, \widehat{\sigma}) > 0$. One can then show that the function $g(\widehat{\xi}, \widehat{\sigma})$ is monotonic over the segment s, that is, $g(\widehat{\xi} = a + b\widehat{\sigma}, \widehat{\sigma})$ is monotonic over $\widehat{\sigma} \in [\sigma_1, \sigma_2]$. As will be used below, this implies that $g(\widehat{\xi}, \widehat{\sigma})$ on the segment s takes its smallest and largest values at the endpoints of s.

To show monotonicity, for the sake of brevity, consider one special but quite broad case, when the segment s falls into the region $\widehat{\xi} > 0$ only. (The general case can be worked out similarly.) Note that in this case, one can write

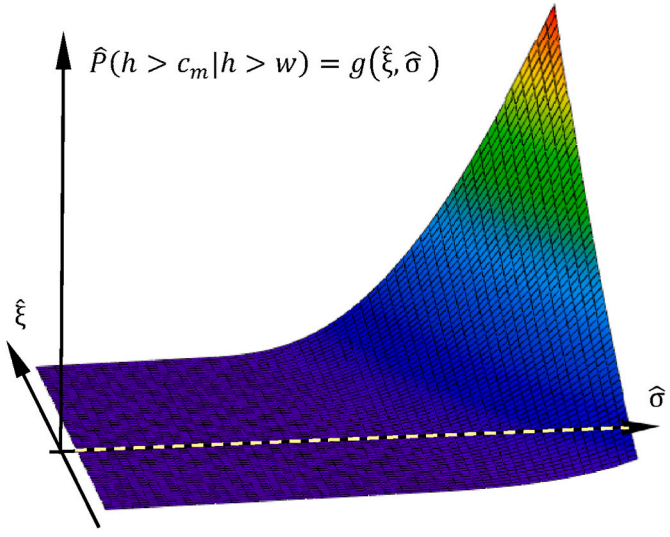

Fig. 26. Estimate of the conditional probability of capsize as a deterministic function of random arguments – estimates of GPD parameters (Belenky et al., 2014)

$$g(\widehat{\xi} = a + b\widehat{\sigma}, \widehat{\sigma}) = \left(1 + \frac{a + b\widehat{\sigma}}{\widehat{\sigma}}\right)^{-1/(a+b\widehat{\sigma})} = (f_1(\widehat{\sigma}))^{-f_2(\widehat{\sigma})} \tag{66}$$

where $f_1(\widehat{\sigma}) = 1 + b + a/\widehat{\sigma} > 1$ and $f_2(\widehat{\sigma}) = 1/(a + b\widehat{\sigma}) > 0$.

The goal is to show that the resulting function in (66) is monotonic as $\widehat{\sigma}\uparrow$ (i.e., $\widehat{\sigma}$ increases). This is demonstrated by considering the following subcases as $\widehat{\sigma}\uparrow$:

$$\begin{array}{l} a < 0,\ b < 0\text{: } f_1\uparrow,\ f_2\uparrow \Rightarrow (f_1)^{f_2}\uparrow \Rightarrow (f_1)^{-f_2}\downarrow \\ a < 0,\ b > 0 : f_1\uparrow,\ f_2\downarrow \Rightarrow (f_1)^{-f_2}\uparrow \\ a > 0,\ b < 0 : f_1\downarrow,\ f_2\downarrow \Rightarrow (f_1)^{f_2}\downarrow \Rightarrow (f_1)^{-f_2}\uparrow \\ a > 0,\ b > 0\text{: } f_1\downarrow,\ f_2\uparrow \Rightarrow (f_1)^{-f_2}\downarrow \end{array} \tag{67}$$

In all the subcases, the function (66) is indeed monotonic as stated.

The simplest way to construct a confidence interval is the boundary method, i.e., taking the upper and lower boundaries of the estimates and substitute them into (65). The method is known to be working for a monotonic function of a single argument, see e.g., section 4.4 of (Bickel and Doksum, 2001). However, the function (65) has two arguments and these arguments are correlated, see equation (57).

Estimates of the shape and scale parameters were assumed as bivariate normal (see subsection 4.4). To account for the correlation between the estimates of shape and scale parameter, Glotzer et al. (2017) construct their confidence interval in transformed coordinates. The correlation of bivariate normal variables can be eliminated by defining a rotation of coordinate system:

$$\widehat{\mathrm{Cov}}(\xi, \sigma) = \begin{pmatrix} \widehat{V}_\xi & \widehat{r}_{\xi\sigma}\left(\widehat{V}_\xi \widehat{V}_\sigma\right)^{0.5} \\ \widehat{r}_{\xi\sigma}\left(\widehat{V}_\xi \widehat{V}_\sigma\right)^{0.5} & \widehat{V}_\sigma \end{pmatrix} \downarrow \begin{pmatrix} \widehat{V}_{\xi 0} & 0 \\ 0 & \widehat{V}_{\sigma 0} \end{pmatrix} = \mathrm{diag}\left(\widehat{V}_{\xi 0}, \widehat{V}_{\sigma 0}\right) \tag{68}$$

where $\widehat{V}_{\xi 0}, \widehat{V}_{\sigma 0}$ are the eigenvalues of $\widehat{\mathrm{Cov}}(\xi, \sigma)$. The boundaries of the confidence interval of the estimates in the transformed coordinates are:

$$\widehat{\xi}^*_{0up,low} = \widehat{E}_\xi \pm Q_N \widehat{V}^{0.5}_{\xi 0}, \quad \widehat{\sigma}^*_{0up,low} = \widehat{E}_\sigma \pm Q_N \widehat{V}^{0.5}_{\sigma 0} \tag{69}$$

A star-superscript means that the boundaries $\widehat{\xi}^*_{0low,up}$ and $\widehat{\sigma}^*_{0up,low}$ need to be computed for the confidence probability $\sqrt{P_\beta}$, when the confidence interval for $\widehat{P}$ is constructed with confidence probability P_β.

In order to use the boundaries (69) in the function (65), the coordinates need to be transformed back to the original frame of references with correlation. A point in the plane $(\widehat{\xi}, \widehat{\sigma})$ is rotated and shifted:

$$\begin{pmatrix} \widehat{\xi} \\ \widehat{\sigma} \end{pmatrix} = \mathbf{T} \cdot \begin{pmatrix} \widehat{\xi} - \widehat{E}_\xi \\ \widehat{\sigma} - \widehat{E}_\sigma \end{pmatrix} + \begin{pmatrix} \widehat{E}_\xi \\ \widehat{E}_\sigma \end{pmatrix} \tag{70}$$

The transformation (70) is applied to four combinations of the boundaries (69):

$$\begin{array}{l} \left(\widehat{\xi}^*_{0up}, \widehat{\sigma}^*_{0up}\right), \left(\widehat{\xi}^*_{0low}, \widehat{\sigma}^*_{0up}\right), \\ \left(\widehat{\xi}^*_{0up}, \widehat{\sigma}^*_{0low}\right), \left(\widehat{\xi}^*_{0low}, \widehat{\sigma}^*_{0low}\right) \end{array} \tag{71}$$

The result are the points:

$$\left(\widehat{\xi}_{up}, \widehat{\sigma}_{up}\right), \left(\widehat{\xi}_{low}, \widehat{\sigma}_{up}\right), \left(\widehat{\xi}_{up}, \widehat{\sigma}_{low}\right), \left(\widehat{\xi}_{low}, \widehat{\sigma}_{low}\right) \tag{72}$$

Boundaries of the confidence interval of the extrapolated probability estimate are computed as min/max of function g over four points (72):

$$\widehat{p}_{low} = \widehat{P}_{low}(h > c_m | h > w) = \min\left(g\left(\widehat{\xi}_{up,low}, \widehat{\sigma}_{up,low}\right)\right) \tag{73}$$

$$\widehat{p}_{up} = \widehat{P}_{up}(h > c_m | h > w) = \max\left(g\left(\widehat{\xi}_{up,low}, \widehat{\sigma}_{up,low}\right)\right) \tag{74}$$

The following observations of (73) and (74) are in place. First, note

that while the points (71) form a rectangle, the rotated points (72) form a rotated rectangle, which is denoted by **R**. In fact, in connection to equation (73), one can write:

$$\begin{aligned}&\min\left(g\left(\widehat{\xi}_{up,low},\widehat{\sigma}_{up,low}\right)\right)\\&=\min(g(\widehat{\xi},\widehat{\sigma}):(\widehat{\xi},\widehat{\sigma})\in\mathbf{R})\end{aligned}\tag{75}$$

and similarly to max in connection to (73):

$$\begin{aligned}&\max\left(g\left(\widehat{\xi}_{up,low},\widehat{\sigma}_{up,low}\right)\right)\\&=\max(g(\widehat{\xi},\widehat{\sigma}):(\widehat{\xi},\widehat{\sigma})\in\mathbf{R})\end{aligned}\tag{76}$$

This is a consequence of the fact proved around equation (66) that the function $g(\widehat{\xi},\widehat{\sigma})$ is monotonic on any segment of parameter values (e.g., the segments can be edges of **R**, implying min/max values at the boundary points (72); similarly for segments crossing the interior of **R**). Second, the confidence interval $(\widehat{p}_{low},\widehat{p}_{up})$ based on the boundaries (73) and (74) will generally be conservative. By the construction above, **R** provides a confidence region for the true parameters (ξ_0,σ_0) with confidence probability P_β. However, (65) is not a one-to-one function. There will be points $(\widehat{\xi},\widehat{\sigma})\notin\mathbf{R}$ such that $g(\widehat{\xi},\widehat{\sigma})$ will fall in $(\widehat{p}_{low},\widehat{p}_{up})$, thus associated with a larger set than **R** resulting in probability values in $(\widehat{p}_{low},\widehat{p}_{up})$ and having a larger probability than P_β. More formally, letting p_0 denote the true probability:

$$\begin{aligned}&P\left(p_0\in\left(\widehat{p}_{low},\widehat{p}_{up}\right)\right)\\&=P\left(g(\xi_0,\sigma_0)\in\left(\widehat{p}_{low},\widehat{p}_{up}\right)\right)>P((\xi_0,\sigma_0)\in\boldsymbol{R})\\&=P_\beta\end{aligned}\tag{77}$$

An alternative is to find a distribution for $\widehat{P}$ using the already defined bivariate normal distribution $\mathrm{PDF}_N(\xi,\sigma)$ with the vector of mean values $(\widehat{\xi},\widehat{\sigma})$ and covariance matrix (57), i.e., to solve a composition problem. The mean value of $\widehat{P}$ is expressed as:

$$\mathbb{E}(\widehat{P})=\iint_{-\infty}^{\infty}g(\xi,\sigma)\mathrm{PDF}_N(\xi,\sigma)d\xi d\sigma\tag{78}$$

and:

$$\mathbb{E}(\widehat{P})\neq g(\widehat{\xi},\widehat{\sigma})\text{ and }\mathbb{E}(\widehat{P})\neq 0\tag{79}$$

The properties of (79) are the result of the nonlinearity of (64). Also, the mean value cannot be zero, because bivariate normal distribution has an infinite support. At the same time, this bivariate normal distribution is an approximation that may not work well for values of GPD estimates that are far from the mean values.

For a complete probabilistic characterization of the extrapolated estimate, consider the cumulative distribution function (CDF). By the definition of CDF:

$$\begin{aligned}&\mathrm{CDF}_P(x)=\mathrm{P}(g(\widehat{\xi},\widehat{\sigma})\le x)\\&=\mathrm{P}((\widehat{\xi},\widehat{\sigma})\in H)\\&=\iint_{(\xi,\sigma)\in H}\mathrm{PDF}_N(\xi,\sigma)d\xi d\sigma\end{aligned}\tag{80}$$

where H is an area in the plane $(\widehat{\xi},\widehat{\sigma})$.

To evaluate the integrals in (80), the area H should be found. From (64), it follows that:

$$g(\xi)\le x\Longleftrightarrow\sigma\le\frac{\xi(c_m-w)}{x^{-\xi}-1},\quad\xi\neq 0\tag{81}$$

To include the case $x=0$, consider the limit and use L'Hôpital's rule to handle an indeterminate form:

$$\lim_{\xi\to 0}\left(\frac{\xi\cdot(c_m-w)}{x^{-\xi}-1}\right)=-\frac{(c_m-w)}{\ln(x)}\tag{82}$$

Combining (81) and (82_ defines the boundary of area H:

$$\sigma_{\lim}(\xi;x>0)=\begin{cases}\dfrac{\xi(c_m-w)}{x^{-\xi}-1}\text{ for }\xi\neq 0\\[2ex]-\dfrac{(c_m-w)}{\ln(x)}\text{ for }\xi=0\end{cases}\tag{83}$$

Substitution of (83) into (80) yields the CDF

$$\mathrm{CDF}_P(x)=\begin{cases}\displaystyle\int_{-\infty}^{\infty}\left(\int_{-\infty}^{\sigma_{\lim}(\xi;x>0)}\mathrm{PDF}_N(\xi,\sigma)d\sigma\right)d\xi\text{ for }x\ge 0\\0\text{ for }x<0\end{cases}\tag{84}$$

The CDF is shown in Fig. 27a. The CDF does not start from zero, which is a consequence of some combinations of the shape and scale parameters leading to a zero value of the estimated conditional probability (65). Differentiation of (84) leads to the probability density function (PDF) of the extrapolated estimate:

$$\begin{aligned}\mathrm{PDF}_P(x)=&\int_{-\infty}^{\infty}\frac{\xi^2x^{-\xi-1}(c_m-w)}{\left(x^{-\xi}-1\right)^2}\\&\times\mathrm{PDF}_N\left(\xi,\frac{\xi\cdot(c_m-w)}{x^{-\xi}-1}\right)d\xi\end{aligned}\tag{85}$$

Consider some properties of this PDF. Its primitive is not continuous, and the CDF may experience a finite jump at $x=0$, so the PDF has an infinite jump. Indeed:

$$\lim_{x\to 0}(\mathrm{PDF}_P(x))=\infty\tag{86}$$

$$\int_0^1\mathrm{PDF}_P(x)dx+\mathrm{CDF}_P(0)=1\tag{87}$$

Furthermore, as x is an estimate of probability:

$$\mathrm{PDF}_P(x)\equiv 0\text{ for }x\notin[0,1]\tag{88}$$

The corresponding PDF is shown in Fig. 27b.

The substitution of $\mathrm{PDF}_N(\widehat{\xi},\widehat{\sigma})$ into (84) completes the consideration of the distribution of the extrapolation estimates. However, as was mentioned when introducing the GPD with equation (50), the scale parameter cannot be negative, while the normal distribution of the parameters' estimates formally supports an infinite domain for both parameters. To avoid possible numerical problems, the bivariate normal distribution may be applied to the logarithm of the scale parameter $\ln(\sigma)$ instead of the scale parameter itself:

$$\mathrm{PDF}_{LN}(\widehat{\xi},\widehat{\sigma})=\mathrm{PDF}_N(\widehat{\xi},\ln(\widehat{\sigma}))\tag{89}$$

The mean value, variance and correlation coefficient of the logarithm of the scale parameter are expressed as:

$$E_{L\sigma}=\ln(E_\sigma);\ V_{L\sigma}=\frac{V_\sigma}{E_\sigma^2};\ r_{\xi L\sigma}=\frac{r_{\xi\sigma}}{E_\sigma}\tag{90}$$

Finally, confidence interval for the extrapolated estimate can be constructed with the numerical evaluation of the relevant quantiles $Q_P(P_\beta)$, leading to:

$$\widehat{P}_{low,up}(h>c_m|h>w)=Q_P\left(\frac{1\mp P_\beta}{2}\right)\tag{91}$$

4.6. Behavior of the tail of the distribution of the capsizing metric

The process of fitting the GPD distribution, described Sections 4.4 and 4.5 is completely driven by data. While universally applicable, the GPD-extrapolation may fail if its shape parameter is estimated to be negative and the right bound happens to be below the target (Pipiras, 2020; Anastopoulos and Spyrou, 2023a). Including physical information through a particular value of the shape parameter improves the reliability of extrapolation e.g., (Weems et al., 2023).

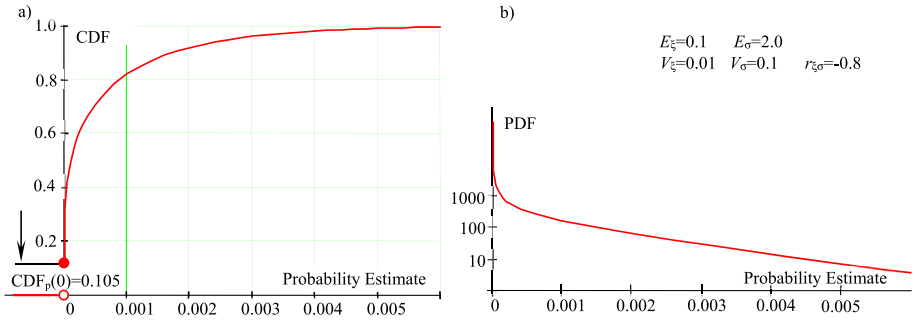

Fig. 27. CFD and PDF of the extrapolated estimate (Belenky et al., 2014).

Glotzer et al. (2017) shows an example where the right bound for pitch motion is selected based on the properties of the pitch restoring. Using the piecewise linear model, Belenky et al. (2019) found that the distribution of peaks of roll angle has a complex tail structure: the tail first becomes heavy around the angle of the maximum of the GZ curve and then becomes light with a right bound near the angle of vanishing stability. As was mentioned in Section 2.8, Glotzer et al., 2024 has demonstrated that the piecewise linear model suggests an exponential tail for the difference between the roll rate at upcrossing and the critical roll rate, i.e., the capsizing metric. Recently published results for the statistical validation of the split-time method (Weems et al., 2023) confirm the exponential character of the capsizing metric. Below is a summary of numerical study of the structure of the tail of the capsizing metric, originally published in Belenky et al. (2018).

The simulations were performed for two of the ONR Topsides Series configurations: tumblehome and flared (Bishop et al., 2005). The simulation tool was SimpleCode, which was briefly introduced in Section 3.1. Three DOFs were modeled: heave, roll and pitch. Nominal values were used for added mass and damping, shown in Table 1. No diffraction was included in the calculations, and forward speed was 6 knots.

The waves were defined by a Bretschneider (1959) spectrum with a significant wave height of 9 m and a modal period of 14 s, which corresponds to Sea State 7. The KG value was adjusted to make capsizing observable and a large-volume sample was produced to compute the critical roll rate and the capsizing metric. The GPD was fitted for a series of thresholds of the capsizing metric, and the calculations where repeated for different wave headings.

Fig. 28a shows the evolution of the shape parameter estimates (with its confidence interval) with the increase of the threshold for beam seas (90 deg. heading). The volume of the sample was 875 hours (1750 records, 30 min each) and contained 3 capsizes, as shown in Table 2. The estimates of the shape parameters start from negative values and indicate a clear tendency to increase, reaching zero around the threshold value of 0.88 rad/s. The zero value is contained within the confidence interval for the rest of the threshold with exception of $w = 0.91$, 0.914 and 0.915 rad/s. This picture appears to be consistent with the hypothesis of an exponential tail of the capsizing metric.

If GPD is fitted to data with a known normal or Rayleigh distribution, i.e. where the tail is known to be exponential, the general picture will be very similar to the one in Fig. 28a. Both normal and Rayleigh distributions contain the square of a variable, with a negative sign. The negative square decreases faster than just a line with negative slope. This circumstance is seen in the GPD as a negative shape parameter for low thresholds. The shape parameter estimate is then expected to stabilize around the zero value. Fig. 28a can be interpreted along these lines.

To observe the effect of stability variation, these calculations were repeated for the 45-degree heading (stern quartering seas), with a forward speed of 6 knots. The sample size was increased to 5000 hours (10,000 30-min records), and contains 206 cases of capsizing. Fig. 28b shows the result, which is dramatically different from the previous, beam seas case. The estimate starts near zero and shows two minima around thresholds 0.65 and 1.01 rad/s.

To find how repeatable this behavior is, the calculations were repeated for the 50-degree heading using an even larger sample of 16,000 hours, where 1093 capsize cases were observed, see Fig. 28c and Table 2. The behavior of the shape parameter estimate did not change, but the confidence interval has shrunk as the volume of the sample has increased.

A further increase of the heading, toward beam seas, is expected to bring the tail to exponential as the influence of the stability variation gets weaker. Fig. 28d contains an estimate of the shape parameters for the 70-degree heading. As in the previous case, the volume of sample was large – 16,000 hours with 1003 capsizing case observed (see Table 2). The behavior of the estimate is very similar to the beam seas result in Fig. 28a, except the stabilization of the shape parameter estimate occurs for a larger threshold value, $w = 1.0$ rad/s, as opposed to the $w = 0.88$ rad/s in the beam seas case.

Thus, the "double minima" topology of the shape parameter estimated for 45° and 50° headings can be attributed to compolex distribution of stability characteristics in waves. Another possible explanation may be related to energy transfer from roll to heave and pitch; similar behavior of the shape parameter has been observed for a tail approximation of roll peaks, see Campbell et al. (2023). However, is this preliminary conclusion applicable to other hull forms?

Fig. 28e is a plot for the shape parameter estimated for ONR Topsides Series flared hull (ONRFL) sailing with a heading of 45°. This hull has the same shape as the ONR tumblehome hull (ONRTH) below the design waterline, but a flared topside similar to conventional destroyers. The sample was also large: 16,000 hours with 53 observed capsizing cases (Table 2). The behavior of the shape parameter estimate is consistent with the hypothesis of an exponential tail. Thus, the "double minima" topology is a result of specific features of stability variation with the ONR tumblehome hull and is not necessarily applicable for other hull configurations.

Table 1
Nominal values for added mass and damping.

Paramters	Values
Ratio of added mass in heave to mass of the ship A_{33}/M	1.0
Ratio of added mass in roll to transversal moment of inertia A_{44}/I_x	0.25
Ratio of added mass in pitch to longitudinal moment of inertia A_{55}/I_y	1.0
Damping in heave, fraction of critical	0.5
Damping in roll, fraction of critical	0.15
Damping in pitch, fraction of critical	0.5

4.7. Fitting exponential tail of distribution for the capsizing metric

The exponential tail of the distribution is one of the particular cases of GPD when the shape parameter is exactly zero, equation (50). The exponential tail has only the scale parameter β (usually used for the exponential distribution instead of σ):

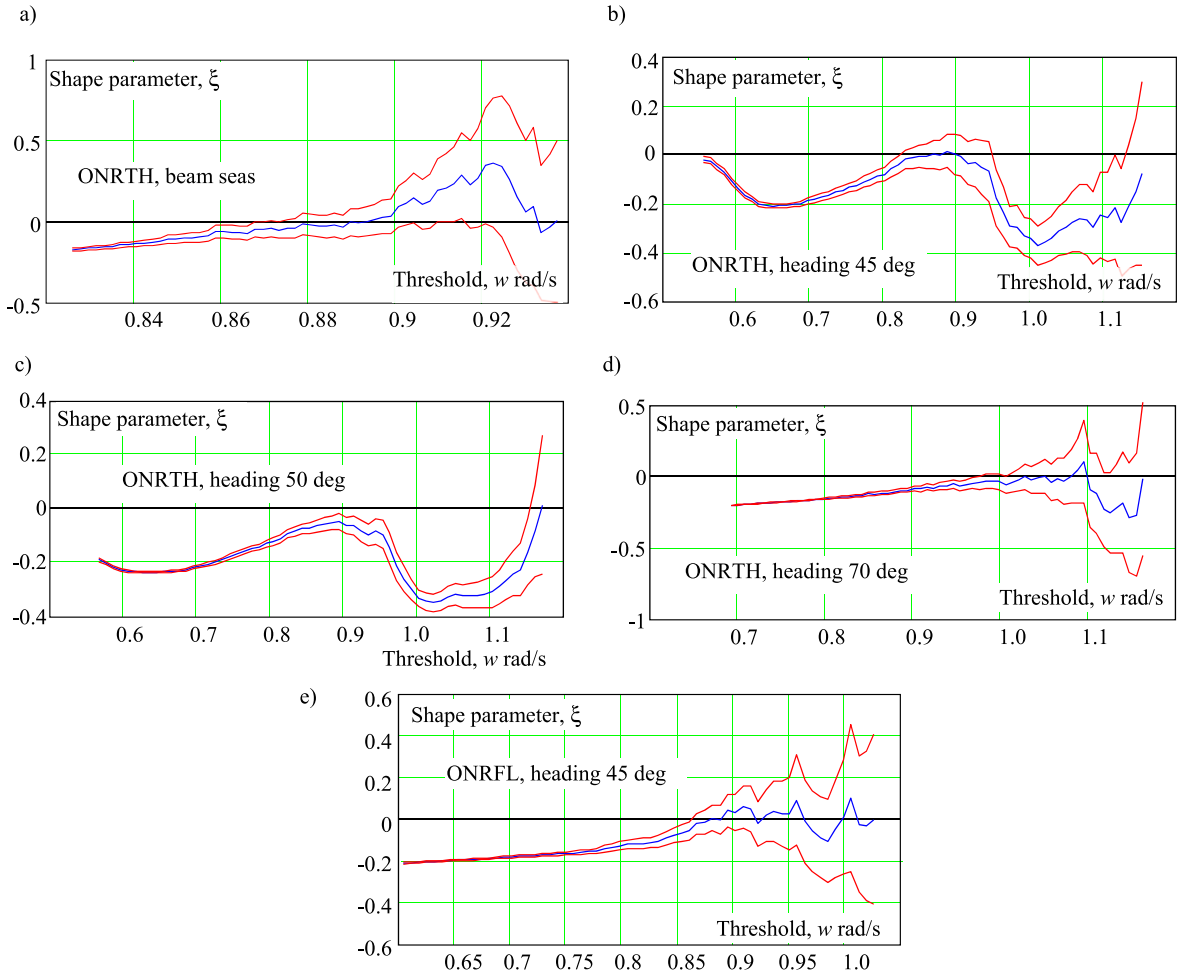

Fig. 28. Behavior of the shape parameter estimates (a) ONRTH, beam seas, KG = 8.35 m; (b) ONRTH, heading 45 deg., KG = 7.85 m; (c) ONRTH, heading 50 deg., KG = 7.85 m; (d) ONRTH, heading 70 deg., KG = 8.00 m (e) ONRFL, heading 45 deg., KG = 8.8 m (Belenky et al., 2018).

Table 2
Conditions for study of shape parameter.

Ship	Heading deg.	KG, m	GM	Numb. caps.	Time, hrs.
TH	45	7.85	1.85	206	5000
TH	50	7.85	1.85	1093	16,000
TH	70	8.00	1.71	1003	16,000
TH	90	8.35	1.36	3	875
FL	45	8.80	0.33	53	16,000

$$\mathrm{PDF}_{EXP}(x) = \begin{cases} \frac{1}{\beta}\exp\left(-\frac{x-w}{\beta}\right) & \text{for} \quad x \geq w \\ 0 \quad \text{for} \quad x < w \end{cases} \tag{92}$$

Being a conditional exponential distribution, the exponential tail inherits all the important properties of the former; in particular, the inversed scale parameter is equal to the mean value of the variable above the threshold, while its variance is equal to its square:

$$\mathbb{E}(x-w) = \beta, \quad \mathrm{Var}(x-w) = \beta^2 \tag{93}$$

Estimating the exponential scale parameter from the data is straightforward:

$$\widehat{\beta} = \frac{1}{N}\sum_{i=1}^{N} z_i \tag{94}$$

where N is the number of data points above a threshold w, and $z_i = h_i -$ w are the sample data points above a threshold w.

Constructing the confidence interval for the estimate of the exponential scale parameter is completed as for any other mean value estimate. The variance of the estimate is computed through the variance of the data points above the threshold:

$$\widehat{V}_z = \frac{1}{N-1}\sum_{i=1}^{N}(z_i - \widehat{\beta})^2, \quad \widehat{\mathrm{V}}_\beta = \frac{\widehat{V}_z}{N} \tag{95}$$

Assuming a normal distribution for the estimate of the exponential scale parameter, the boundaries of its confidence interval are:

$$\widehat{\beta}_{up,low} = \widehat{\beta} \pm Q_N \widehat{V}_\beta^{0.5} \tag{96}$$

where Q_N is the standard normal quantile; for confidence probability $P_{\beta} = 0.95$, $Q_N = 1.96$.

Fitting an exponential tail generally follows the same steps as the GPD approximation, including the selection of an appropriate threshold. Two methods for the threshold selection for the capsizing metric were described in (Belenky et al., 2018a): Goodness-of-fit Test and Prediction Error Criterion. The former was later retired due to ambiguity of setting the level of significance, but both these methods where used in the statistical validation effort of Weems et al. (2023). Both methods are described here.

The goodness-of-fit method was developed by Stephens (1974) by modifying the traditional Kolmogorov-Smirnov (KS) goodness-of-fit test for the exponential distribution and for the case when the parameter is unknown and needs to be estimated. The fit test is based on the

maximum distance between the theoretical (exponential in this case) and observed distributions. The null hypothesis H_0 is such that the observed data follows the theoretical distribution.

To use the goodness-of-fit test, the data above each candidate threshold is sorted in ascending order $y_i = \text{sort}(z_i)$, $i = 1, \ldots N$. The theoretical CDF is expressed as:

$$\text{CDF}_i = 1 - \exp\left(-\frac{y_i}{\widehat{\beta}}\right) \tag{97}$$

The maximum distance between the observed and theoretical distribution:

$$D = \max\{D^+, D^-\}, D^+ = \max_{i=1,\ldots,N}\left|\frac{i}{N} - cdf_i\right|, D^- = \max_{i=1,\ldots,N}\left|cdf_i - \frac{i-1}{N}\right| \tag{98}$$

The test statistic for the null hypothesis is defined as:

$$D^* = \left(D - \frac{0.2}{N}\right)\left(\sqrt{N} + 0.26 + \frac{0.5}{\sqrt{N}}\right) \tag{99}$$

The critical values for D^* are available from Stephens (1974) and are listed in Table 3 for several p-values, the probability that the observed difference is caused by random reasons (if this probability is too small, a systematic difference is observed and the null hypothesis has to be rejected).

For each of the candidate thresholds, the test statistic D^* is computed. The p-value is found from Table 3. Since Table 3 has critical values for only a limited number of probabilities, the resulting p-value is taken as the number whose critical value is the largest but still smaller than computed test statistics D^*; e.g. for $D^* = 0.8$, $p = 0.3$.

A final threshold is selected as the largest w above which all the thresholds have their associated p-values exceeding the accepted significance level. A significance level of 5 % seems reasonable at first glance, but it should be larger for the extrapolation to work, roughly 10 % or above. That is, the exponential distribution provides an adequate fit of the thresholds above the selected one. A numerical example of the selected thresholds for two datasets are summarized in Table 4 where the results look consistent in terms of the selected threshold. The slight increase of the selected threshold with the increase of the significance level can be explained by the more stringent requirement for the goodness-of-fit associated with the larger p-value.

A prediction error criterion for selecting a threshold for the extrapolation with an exponential distribution can be found in Mager (2015). This method is based on the following principle. Let $y_n \leq \ldots \leq y_1$ be the upper order statistics of the observations h_i, i.e., the result of sorting these observation in descending order:

$$\overrightarrow{y} = \text{sort}_{\text{desc}}\left(\overrightarrow{h}\right) \Rightarrow y_n \leq \ldots \leq y_1 \tag{100}$$

A threshold w will be chosen as $w = y_{k+1}$ and thus is associated with the $(k+1)^{th}$ largest observation and the index $(k+1)$. For this $w = y_{k+1}$, let $s_i = y_i - w, i = 1, \ldots, k$.

The focus of the method is on the so-called mean squared prediction error defined as:

$$\Gamma(k) = \frac{1}{k}\sum_{i=1}^{k}\mathbb{E}\left(\frac{(\widehat{s}_i - \mathbb{E}s_i)^2}{\text{Var}(s_i)}\right) \tag{101}$$

where $\widehat{s}_i$ is the estimated value of s_i according to the exponential model.

Table 3
Critical value of D^*.

Parameter	Value					
p-value	0.01	0.025	0.05	0.10	0.15	0.20
D^*	1.308	1.190	1.094	0.990	0.926	0.880
p-value	0.25	0.30	0.35	0.40	0.45	0.50
D^*	0.835	0.795	0.766	0.736	0.710	0.685

Table 4
Numerical example of threshold selection with goodness-of-fit test.

p-value	0.1	0.2	0.3	0.4	0.5
w, rad/s, Data set 1	0.521	0.534	0.534	0.699	0.699
w, rad/s, Data set 2	0.657	0.666	0.666	0.666	0.670

The basic idea behind the threshold selection is to choose k, which minimizes an estimate of $\Gamma(k)$.

To estimate $\Gamma(k)$, it is first expressed as:

$$\Gamma(k) = \frac{1}{k}\sum_{i=1}^{k}\mathbb{E}\left(\frac{(\widehat{x}_{i,k} - x_{i,k})^2}{\text{Var}(x_{i,k})}\right) + \frac{2}{k}\sum_{i=1}^{k}\frac{\text{Cov}(\widehat{x}_{i,k}, x_{i,k})}{\text{Var}(x_{i,k})} - 1 \tag{102}$$

The equality is proved in Mager (2015), Lemma 4.2. The derivation is also available from Campbell et al. (2023). The estimator of $\Gamma(k)$ is then defined as:

$$\widehat{\Gamma}(k) = \frac{1}{k}\sum_{i=1}^{k}\frac{(\widehat{x}_{i,k} - x_{i,k})^2}{\widehat{\text{Var}}(x_{i,k})} + \frac{2}{k}\sum_{i=1}^{k}\frac{\widehat{Cov}(\widehat{x}_{i,k}, x_{i,k})}{\widehat{\text{Var}}(x_{i,k})} - 1 \tag{103}$$

The index $\widehat{k}$ for the threshold selection is chosen as that which minimizes $\widehat{\Gamma}(k)$ over some range of values of k. Mager (2015) suggests using the range $[\max(40, 0.02N), 0.2N]$, where N is the total number of points available.

To conclude the description of the method, it is necessary to specify the various quantities in the definition of $\widehat{\Gamma}(k)$. Under the exponential model, the distributions of the order statistics s_i are well-known e.g., Example 4.1.5 in (Embrechts et al., 2013). The details on a derivation are also available from Campbell et al. (2023) where a similar prediction error function for Pareto distribution is described. The result is

$$\text{Var}(s_i) = \beta^2\sum_{j=i}^{k}\frac{1}{j^2} \approx \beta^2\frac{1}{k}\left(\frac{k+1}{i} - 1\right) \tag{104}$$

This approximation is used by Mager (2015). This quantity can then naturally be estimated through

$$\widehat{\text{Var}}(s_{i,}) = \widehat{\beta}^2\frac{1}{k}\left(\frac{k+1}{i} - 1\right) \tag{105}$$

where $\widehat{\beta}$ is defined in equation (94).

The estimator $\widehat{s}_i$ of s_i is defined as follows. One can think of s_i as the $(1 - i/(k+1))^{th}$ quantile of the exponential distribution. But for this distribution, this quantile is $-\beta\ln(i/(k+1))$, which suggests using:

$$\widehat{s}_i = -\widehat{\beta}\ln\left(\frac{i}{k+1}\right) \tag{106}$$

With details available from Campbell et al. (2023), the following is the result

$$\text{Cov}(\widehat{s}_i, s_{i,}) \approx \frac{\beta^2}{k}\left(\ln\left(\frac{i}{k+1}\right)\right)^2 \tag{107}$$

This suggests the use of:

$$\widehat{\text{Cov}}(\widehat{s}_i, s_{i,}) = \frac{\widehat{\beta}^2}{k}\left(\ln\left(\frac{i}{k+1}\right)\right)^2 \tag{108}$$

Substituting these quantities into the definition of $\widehat{\Gamma}(k)$ from equation (103) leads to the expression:

$$\widehat{\Gamma}(k) = \widehat{\beta}^{-2}\sum_{i=1}^{k}\left(\frac{k+1}{i} - 1\right)^{-1}\left(s_i + \widehat{\beta}\ln\left(\frac{i}{k+1}\right)\right)^2 + \frac{2}{k}\sum_{i=1}^{k}\left(\frac{k+1}{i} - 1\right)^{-1}\left(\ln\left(\frac{i}{k+1}\right)\right)^2 - 1 \tag{109}$$

This also appears in Mager (2015), at the bottom of p. 64. A

numerical example of $\widehat{\Gamma}(k)$ is in Fig. 29.

Once the threshold has been selected, the calculation of the extrapolated estimate and its confidence interval is straightforward:

$$\widehat{P}(h > c_m | h > w) = \widehat{P}(h > c) = \exp\left(-\widehat{\beta}^{-1}(c - w) \right) \tag{110}$$

$$\widehat{P}_{low,up}(h > c_m | h > w) = \exp\left(-\widehat{\beta}^{-1}_{low,up}(c - w) \right) \tag{111}$$

A comparison of the rates of capsizing estimated with different methods will be presented in Section 5.

5. Estimation of rate of capsizing

5.1. Non-rare problem and the rate of capsizing estimate

Equation (23) describes a random event of capsizing as an upcrossing of an intermediate level ϕ_{m0} by a roll motion process when the metric (52) exceeds its target value c_m. The later was referred as the rare problem, while the former was identified as the non-rare problem. This terminology reflects the notion that upcrossing events are readily observed in normal simulation, while capsizing is not.

Estimating the rate of upcrossing events is straightforward:

$$\widehat{r}_U = \frac{N_U}{\sum_{i=1}^{N_R} T_{Ri}} \tag{112}$$

where T_{Ri} is a duration of i^{th} record, and N_U is the number of upcrossing events. Alternative methods are described in Wandji et al. (2024).

Defining the number of upcrossing events deserves some discussion. The total number of observed upcrossing events of the intermediate level ϕ_{m0} is not relevant, as the extreme value theory for the rare problem requires independent data, see Subsection 4.2. The declustering procedure, described in Subsection 4.3, selects independent upcrossing events. The number of independent upcrossings is equal to the number of clusters in the data.

The second extreme-value theorem is a main vehicle for the rare problem; a tail of the capsizing metric distribution was fitted. The threshold, where the tail starts, was found as a part of the tail fitting procedure, described in Sections 4.4 for GPD and 4.7 for the exponential tail. Not every capsizing metric value, corresponding to a selected upcrossing event, is used for fitting the tail – only those that exceed the threshold.

Thus, the number of upcrossing events in equation (112) is equal to N, the number of capsizing metric data points above the selected threshold w, as defined for the equation (50):

$$N_U = N \tag{113}$$

This threshold w selected for fitting the tail now serves as a separation point between the non-rare and rare problems. Crossing this threshold by the capsizing metric data is still the observable event, while extreme properties can be claimed for the data above this threshold.

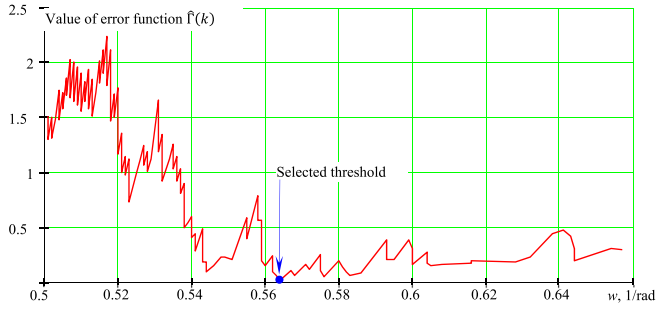

Fig. 29. Error function for threshold selection with the predication error criterion.

The complete estimate for the rate of capsizing is expressed as:

$$\widehat{r}_C = \frac{N}{\sum_{i=1}^{N_R} T_{Ri}} \widehat{P}(h > c_m | h > w) \tag{114}$$

where h and c_m are defined in equation (52) and is determined by one of the procedures described in Sections 4.3 or 4.7.

5.2. Uncertainty of the capsizing rate estimate

The capsizing rate estimate (114) is a product of two estimates: the rate of upcrossings of the threshold w and the probability of exceedance of the extrapolation target c_m, associated with a capsizing event. Assuming independence of the estimates, a confidence interval can be constructed by multiplying the boundaries of the components:

$$\begin{aligned} \widehat{r}_{C,low} &= \widehat{r}_{U,low} \cdot \widehat{P}_{low}(h > c_m | h > w), \\ \widehat{r}_{C,up} &= \widehat{r}_{U,up} \cdot \widehat{P}_{up}(h > c_m | h > w), \end{aligned} \tag{115}$$

where $\widehat{P}_{low,up}(h > c_m | h > w)$ are the boundaries of confidence interval for the rare problem defined with equations (73), (74), (91) and (111), while $\widehat{r}_{U,low}$ and $\widehat{r}_{U,up}$ are the boundaries of the confidence interval for the upcrossing rate through the threshold w, i.e. the non-rare problem.

As a boundary of the confidence interval is a product, the confidence probability for each of the boundaries has to be considered as $P_{\beta 1} = \sqrt{P_\beta}$. The counting of upcrossing events is essentially a Bernoulli trial (at each time instant, an upcrossing event either occurs or not), so the crossing rate estimate follows binomial distribution with the parameter:

$$\widehat{p}_U = \widehat{r}_U \Delta t \tag{116}$$

where Δt is the time increment in the numerical simulation of ship motions. The boundaries of the confidence interval are expressed through the appropriate quantiles of binomial distribution, while alternative methods are available from Wandji et al. (2024):

$$\begin{aligned} \widehat{r}_{U,low} &= Q_B\left(\frac{1 - P_{\beta 1}}{2}; \widehat{p}_U, N_U \right) \\ \widehat{r}_{U,Up} &= Q_B\left(\frac{1 + P_{\beta 1}}{2}; \widehat{p}_U, N_U \right) \end{aligned} \tag{117}$$

For boundaries of confidence interval for GPD-extrapolated estimate computed with equations 71 and 72, the confidence probability has to be considered as $P_{\beta 2} = \sqrt{P_{\beta 1}} = \sqrt[4]{P_\beta}$.

5.3. Numerical example of estimation of capsizing rate

Numerical example of estimation of capsizing rate was computed with SimpleCode for ONR Topside Series tumblehome configuration (Bishop et al., 2005). The significant wave height was 9 m, modal period was 14 s, forward speed was 6 knots in stern quartering seas (heading 45°), GM value was set to 2.2 m. Simulation was performed with 3-DOF (heave, roll, pitch). The dynamic characteristics for added mass and damping are provided in Table 1.

The data from this example has been used for illustrations throughout this paper. Figs. 11 and 12 show an episode of pure loss of stability, leading to a large roll angle, and a small difference between roll rate at the instant of upcrossing and the critical roll rate. The declustering procedure for one of the records was illustrated in Fig. 20. The simulations consist of 200 30-min records, providing 800 values of capsizing metric after the declustering procedure was applied.

Fig. 21 shows the negative log likelihood computed for a threshold that was close to the value that was selected. Fig. 22 through 25 depict selection of the threshold for GPD, using all four considered procedures. Table 4 includes the results of the threshold selection for the exponential tail with the goodness-of-fit test, while Fig. 29 illustrates the application of the prediction error criterion. Finally, Fig. 30a contains the rate of

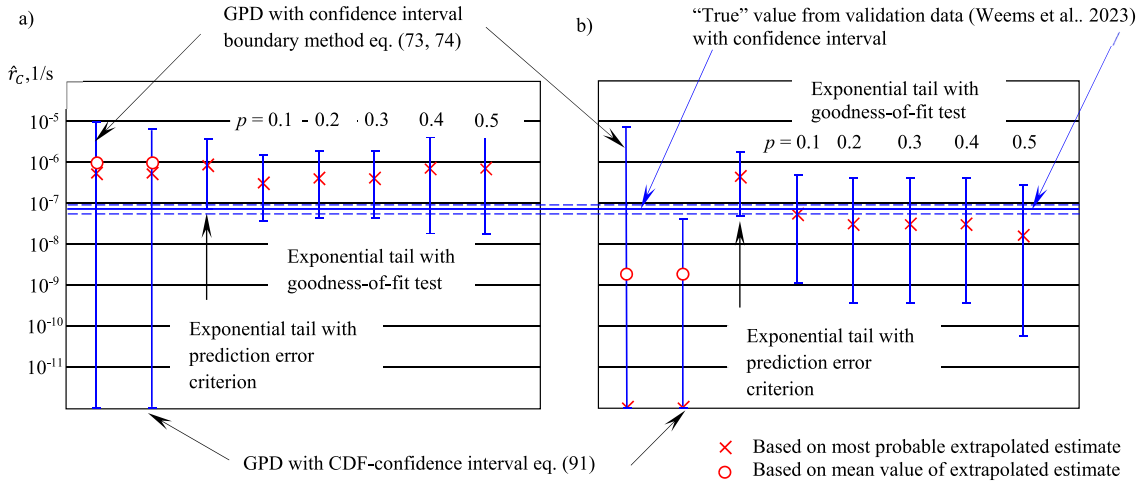

Fig. 30. Estimates of capsizing rate in comparison with the "true" value from validation data (Weems et al., 2023) with confidence interval; (a) data set 1 (b) data set 2.

capsizing estimated with different methods: GPD tail with two techniques for computing the confidence interval (the extrapolated estimate remains the same) and two methods for selecting the threshold for the exponential tail (the capsizing rate changes with extrapolated estimate).

To see the influence of data variability, a second data set has been generated; the quantity of data was the same with 800 independent capsizing metric values. The results of the threshold selection for the exponential tail with goodness-of-fit method is for the second data set was placed in Table 4. The estimates of the capsizing rates for the second dataset are shown in Fig. 30b. A "true" capsizing rate value was added to Fig. 30 from validation data (Weems et al., 2023). Confidence intervals of all of the results captures the "true" value with exception of the GPD case with confidence interval (91) in Fig. 30b.

No influence of the data variation on the threshold selection is observed in Table 4. More difference is evident between the two datasets in Fig. 30. The most obvious influence of the data variation is in the GPD extrapolation. The capsizing rate estimates based on GPD and exponential tail extrapolation are consistent for the first data set in Fig. 30a. The capsizing rate, estimated with GPD for the second dataset, shown in Fig. 30b, has zero for the most probable value, while the mean recovers a non-zero value. It is an illustration of one of the "pitfalls" of GPD – the shape parameter is too small and the right bound is located before the extrapolated target. This is a result of the natural variability of the data, as warned by Pipiras (2020), Anastopoulos and Spyrou (2023a).

At the same time, all data variability influences are well within the confidence interval for the exponential tail extrapolation, indicating the robustness the approximation. As expected, the GPD-based estimate (when successful) has wider confidence interval, compared to the exponential tail: any physics-informed extrapolation method is expected to have less uncertainty. This is consistent with observations described in the previous works, e.g., (Glotzer et al., 2017). However, the upper boundary of GPD-based estimate computed with its CDF (Fig. 30a) is not significantly more conservative compared to the exponential tail. The "boundary" method (73, 74) provided more conservatism, but this is expected. The most consistent results were achieved with the estimate based on the exponential tail and the prediction error criterion for the threshold selection. These results are in-line with the validation and performance study of split-time method for capsizing probability described by Weems et al. (2023).

6. Summary

The significant length of this paper may be justified by the complexity of the subject of the probability of capsizing and the intention to track the development of the split-time method from reduced-order models of nonlinear roll to physics-informed numerical application. Some key points regarding the method are listed below.

The capsizing of an intact ship in irregular ocean waves is a rare event that can be modeled as Poisson flow. Poisson flow provides a relationship between probability and time of exposure. Evaluation of capsizing rate is sufficient in order to compute the probability of capsizing over a given period of time.

A piecewise linear dynamical system is introduced as a single degree-of-freedom ordinary differential equation with three-range piecewise linear restoring. The piecewise linear system is a combination of attractor and repeller and is configured to have two stable equilibria ("upright" and "upside-down") and one unstable equilibrium between them.

The piecewise linear system models the very essence of the capsizing — a transition to motion around the upside-down equilibrium. While quite exotic for ship dynamics application, the piecewise linear system is still physical. A force does not have to be smooth (or even continuous, e.g., dry friction) in mechanics. Velocity and displacement being primitives of acceleration are smooth in a dynamical system with piecewise linear restoring.

The piecewise linear dynamical system is essentially nonlinear, with its nonlinearity concentrated in a single point. The piecewise linear system has most of the nonlinear properties of the single DOF equation of roll motion with a smooth roll restoring (GZ) curve. The piecewise linear system can therefore be used as a qualitative reduced-order model of large roll motions, and the transition to motion near the "upside down" equilibrium is a qualitative description of the capsizing of a ship in waves.

The piecewise linear dynamical system allows an analytical solution for the rate of capsizing. It is constructed from two components. The first component is a rate of upcrossing of a boundary between the two intervals. The second component is a probability of exceedance of a critical value by the roll rate at the instant of upcrossing. The critical value is expressed analytically from the solution for the repeller part of the piecewise linear dynamical system. The roll rate at the instant of upcrossing follows a Rayleigh distribution, so the probability of exceedance can be expressed explicitly.

The piecewise linear dynamical system may account for additional factors such as gusty wind, drift and the variation of stability in waves. These additional factors are reflected in probabilistic characteristics of the critical roll rate as well as in the rate of upcrossing through characteristics of the roll motion.

The study of capsizing, using the piecewise linear system, inspires

the formulation of a principle of separation of a complex probabilistic problem into two less complex ones. The non-rare problem is calculation of rate of upcrossings over a boundary that may be set low enough to observe and count these upcrossings. The rare problem is the evaluation of probability of capsizing after upcrossing.

The split-time method is a result of recasting of ideas, formulated for the piecewise linear system, for a numerical simulation tool. An intermediate level for the roll angle is introduced to play the role of the boundary of the two ranges in the piecewise linear system. A critical roll rate is computed at each instant of upcrossing of the intermediate level. These calculations are performed by systematically perturbing the roll rate at the instant of upcrossing. The perturbed simulations are started at the instant of upcrossing and run for a short duration of time. The initial roll rate is increased until capsizing is observed. The perturbation simulations are performed for each upcrossing, creating a dataset of the observed and critical roll rates at the instants of upcrossing.

A metric of the likelihood of capsizing is defined as the difference between the critical roll rate and the observed roll rate at each instant of upcrossing. The smaller this difference is, the more likely capsizing is to occur. As the metric is computed through simulation forward into the future, it includes the physical behavior of large roll motion and the changing stability in waves. Whatever phenomena may occur, they are included in the perturbation simulations. In a sense, the capsizing metric dataset contains information on "what would have happened if …".

As the capsizing metric dataset contains information on potential capsizing, the extrapolation of this data can produce an estimate of probability of capsizing, which is the solution for the rare problem. The non-rare problem is the estimation of the rate of upcrossing of the intermediate level.

Extrapolation of the capsizing metric is approached through the application of extreme value theory, which states that the tail of a distribution above a large enough threshold can be approximated with a Generalized Pareto Distribution (GPD). The shape and scale parameters of the GPD are found with the log-likelihood method. The large-enough threshold can be found by stabilization of the shape parameter, which is an indicator of the applicability of extreme value theory, or by a minimization of difference between the GPD and the observed distribution.

The extrapolation of the data with GPD may fail due to the natural variability of the data. If the shape parameter estimate is negative, it introduces a bound of the distribution that may be below the target of extrapolation, leading to a zero-answer.

The extrapolation may become physics-informed by imposing a condition for the shape parameter, based on physical consideration, rather than estimating the shape parameter from the data. A distribution of the capsizing metric of piecewise linear system has an exponential tail, i.e., the shape parameter is zero. Large-volume numerical simulations have a shape-parameter estimate approaching zero, as capsizing becomes observable, i.e. did not reject the exponential tail of the capsizing metric. The extrapolation of the capsizing metric with exponential tail follows the same steps as the GPD tail extrapolation, being a special case of it, but is more robust and provide less statistical uncertainty compare to GPD.

7. Conclusions

Physics-informed extrapolation unlocks the full power of extreme value theory and allows the extension of data-driven approach towards estimating a probability of the occurrence of a rare capsizing event that was not observed in available data. Information of these possible, but not-yet-observed rare capsizing events can be extracted from a dynamical system through finite perturbation. The differences between unperturbed and perturbed, leading-to-capsizing roll rate values makes a metric of likelihood of capsizing at a particular moment of time. The computed instances of the metric make new data to which the extreme value theory can be applied.

A reduced-order model of roll motions with piecewise linear restoring provides a simple but qualitatively valid model of capsizing as a transition to motion near the "upside-down" equilibrium. The piecewise linear model allows closed-form solution for the probability of capsizing and uncovers a type of exponential tail for the distribution of the capsizing metric. The physical information on capsizing is used twice in the described approach: to create the data and to characterize its extreme behavior.

The split-time method may be useful for the extrapolation of the response of dynamical systems when phenomena associated with a large-magnitude response is not normally present in the data. In addition to capsizing, broaching-to and water-on-deck problems may be considered as potential candidates for the application of the split-time method. An attempt to study broaching in irregular wave with perturbation is described in Belenky et al. (2023), while the application of split-time method for water-on-deck problem will require perturbations to be performed with unsteady Reynolds-averaged Navier-Stokes (URANS) simulations.

CRediT authorship contribution statement

Vadim Belenky: Conceptualization, Data curation, Formal analysis, Investigation, Methodology, Writing – original draft. **Kenneth M. Weems:** Data curation, Investigation, Methodology, Software, Validation, Writing – review & editing. **Woei-Min Lin:** Project administration, Supervision, Writing – review & editing. **Vladas Pipiras:** Formal analysis, Investigation, Methodology, Writing – review & editing. **Themistoklis P. Sapsis:** Formal analysis, Investigation, Methodology, Writing – review & editing.

Declaration of competing interest

The authors declare that they have no known competing financial interests or personal relationships that could have appeared to influence the work reported in this paper.

Data availability

Data will be made available on request.

Acknowledgements

The work described in this paper has been funded since 2006 by the Office of Naval Research (ONR) under Dr. Patrick Purtell, Dr. Ki-Han Kim, and Dr. Thomas Fu. This work was also supported by the Naval Surface Warfare Center Carderock Division (NSWCCD) Independent Applied Research (IAR) program under Dr. Jack Price.

Besides the ONR funding, the participation of Prof. Sapsis was also facilitated by the NSWCCD Summer Faculty Program, while the participation of Prof. Pipiras was alsofacilitated by the NSWCCD Summer Faculty and Sabbatical Programs, both of which were also managed by Dr. Jack Price.

Over the years of the research, many colleagues have influenced and contributed to our work. The authors would like acknowledge Dr. Art Reed, Mr. Tim Smith, Mr. Brad Campbell (NSWCCD, David Taylor Model Basin), Prof. Kostas Spyrou (National Technical University of Athens, Greece), Prof. Naoya Umeda (University of Osaka, Japan), Prof. Pol Spanos (Rice University) and the late Prof. Ross Leadbetter (University of North Carolina at Chapel Hill).

References

Alford, L.K., Troesch, A.W., 2009. Generating extreme ship responses using non-uniform phase distributions. Ocean Eng. 36 (9–10), 641–649.

Anastopoulos, P.A., Spyrou, K.J., 2019. Evaluation of the critical wave groups method in calculating the probability of ship capsize in beam seas. Ocean Eng. 187, 106213.

Anastopoulos, P.A., Spyrou, K.J., 2022. Extrapolation over Significant Wave Height with the Aid of Stochastic Wave Groups Theory. Proc. 18th Intl. Ship Stability Workshop, Gdansk, Poland, pp. 125–136.

Anastopoulos, P.A., Spyrou, K., 2023. An efficient formulation of the critical wave groups method for the assessment of ship stability in beam seas. In: Spyrou, K., Belenky, V., Katayama, T., Bačkalov, I., Francescutto, A. (Eds.), Contemporary Ideas on Ship Stability – from Dynamics to Criteria, pp. 157–174. Springer Series Fluid Mechanics and Its Application ISBN 978-3-031-16328-9.

Anastopoulos, P.A., Spyrou, K., 2023a. Effectiveness of the generalized Pareto distribution for characterizing ship tendency for capsize. In: Belenky, V., Katayama, T., Bačkalov, I., Francescutto, A. (Eds.), *Contemporary Ideas On Ship Stability – from Dynamics To Criteria*, Spyrou, K., pp. 245–263. Springer Series Fluid Mechanics and Its Application ISBN 978-3-031-16328-9.

Anastopoulos, P.A., Spyrou, K., 2023b. Extrapolation of ship capsize probability over significant wave height: foundation on wave groups theory. this issue Ocean Eng. 281, 18 (114766) this issue.

Anastopoulos, P.A., Spyrou, K.J., Bassler, C.C., Belenky, V., 2016. Towards an Improved Critical Wave Groups Method for the Probabilistic Assessment of Large Ship Motions in Irregular Sea *Probabilistic Engineering Mechanics*, vol. 44, pp. 18–27.

Bassler, C.C., Dipper, M.J., Melendez, M., 2019. Experimental ship dynamic stability assessment using wave groups. In: Belenky, V., Spyrou, K., van Walree, F., Neves, M. A.S., Umeda, N. (Eds.), Chapter 30 of Contemporary Ideas on Ship Stability. Risk of Capsizing. Springer, pp. 507–520. ISBN 978-3-030-00514-6.

Belenky, V.L., 1989. A new method of statistical linearization in severe rolling and capsizing problem. In: Proc. Scientific Methodological Seminar on Ship Hydrodynamics, *SMSSH'89* Bulgarian Ship Hydrodynamics Center (BSHC), Varna, Bulgaria, vol. 2, pp. 39.1–39.6.

Belenky, V.L., 1993. A capsizing probability computation method. J. Ship Res. 37 (3), 200–207.

Belenky, V.L., 1994. Piecewise linear methods for the probabilistic stability assessment for ship in a seaway. In: Proc. 5th Intl. Conf. On Stability of Ships and Ocean Vehicles, (STAB 1994), vol. 5. Melbourne, Florida, USA.

Belenky, V.L., 1995. On the dynamics of piecewise linear system. In: *Proc. Intl. Symp. On Ship Safety In a Seaway: Stability, Maneuverability, Nonlinear Approach In Memory Of Professor Sevastianov,* Kaliningrad, Russia, vol. 1, pp. 6.1–6.8.

Belenky, V.L., 1997. Capsizing risk function estimation due to pure loss of stability in quartering seas. In: *Proc. 6th Intl. Conf. On Stability Of Ships And Ocean Vehicles (STAB 1997),* Varna, Bulgaria, vol. 1, pp. 315–322.

Belenky, V.L., 2000. Piecewise linear approach to nonlinear ship dynamics. In: Vassalos, D., Hamamoto, M., Papanikolaou, A., Molyneux, D. (Eds.), Contemporary Ideas on Ship Stability. Elsevier, pp. 149–160. ISBN 0-08-043652-8.

Belenky, V.L., 2000a. Piecewise linear approach to probabilistic stability in quartering seas. In: Proc. 7th Intl. Conf. On Stability of Ships and Ocean Vehicles, A. STAB 2000, Launceston, Tasmania, Australia, pp. 503–510.

Belenky, V., Weems, K., Campbell, B. and V. Pipiras, 2014. Extrapolation and validation aspects of the split-time method. In: Proc. 30th Symp. Naval Hydrodynamics, Hobart, Tasmania, Australia.

Belenky, V.L., Sevastianov, N.B., 2007. Stability and Safety of Ships: Risk of Capsizing, second ed. SNAME, Jersey City. ISBN 0-939773-61-9.

Belenky, V., Weems, K.M., 2008. Procedure for probabilistic evaluation of large amplitude roll motions. In: Proc. Osaka Colloquium on Seakeeping and Stability of Ships, pp. 213–220. Osaka, Japan.

Belenky, V., Weems, K.M., 2008a. Probabilistic qualities of stability change in waves. In: Proc. 10th Intl. Ship Stability Workshop, Daejon, Korea, pp. 95–108.

Belenky, V., Weems, K.M., 2019. Dependence of Roll and Roll Rate in Nonlinear Ship Motions in Following and Stern Quartering Seas. In: Belenky, V., Spyrou, K., van Walree, F., Neves, M.A.S., Umeda, N. (Eds.), *Contemporary Ideas On Ship Stability. Risk Of Capsizing*. Springer, pp. 455–473. ISBN 978-3-030-00514-6.

Belenky, V., Weems, K.M., Lin, W.M., 2008. Numerical procedure for evaluation of capsizing probability with split time method. In: Proc. 27th Symp. Naval Hydrodynamics, Seoul, Korea.

Belenky, V., Reed, A.M., Weems, K.M., 2011. Probability of capsizing in beam seas with piecewise linear stochastic GZ curve. In: Neves, M.A.S., Belenky, V., de Kat, J.O., Spyrou, K., Umeda, N. (Eds.), *Contemporary Ideas On Ship Stability*. Springer, pp. 531–554. ISBN 978-94-007-1481-6.

Belenky, V., Weems, K.M., Bassler, C.C., Dipper, M.J., Campbell, B., Spyrou, K., 2012. Approaches to rare events in stochastic dynamics of ships. Probabilist. Eng. Mech. 28, 30–38.

Belenky, V., Weems, K., Lin, W.M., 2016. Split-time method for estimation of probability of capsizing caused by pure loss of stability. Ocean Eng. 122, 333–343.

Belenky, V., Weems, K., Pipiras, V., Glotzer, D., Sapsis, T., 2018. Tail structure of roll and metric of capsizing in irregular waves. In: Proc. 32nd Symp. Naval Hydrodynamics, Hamburg, Germany.

Belenky, V., Weems, K., Pipiras, V., Glotzer, D., 2018a. Extreme-value properties of the split-time metric. In: Proc. 13th Intl. Conf. On Stability of Ships and Ocean Vehicles (STAB 2018) (Kobe, Japan).

Belenky, V., Glotzer, D., Pipiras, V., Sapsis, T., 2019. Distribution tail structure and extreme value analysis of constrained piecewise linear oscillators. Probabilist. Eng. Mech. 57, 1–13.

Belenky, V., Weems, K.M., Spyrou, K., Pipiras, V., Sapsis, T., 2023. Modeling broaching-to and capsizing with extreme value theory. In: Spyrou, K., Belenky, V., Katayama, T., Bačkalov, I., Francescutto, A. (Eds.), Contemporary Ideas on Ship Stability – from Dynamics to Criteria. Springer, pp. 435–457. ISBN 978-3-031-16328-9.

Bickel, J.P., Doksum, K.A., 2001. Mathematical Statistics: Basic Ideas and Selected Topics, vol. 1. Prentice-Hall, Upper Saddle River, NJ. ISBN 0-13-850363-X.

Bishop, R.C., Belknap, W., Turner, C., Simon, B., Kim, J.H., 2005. Parametric Investigation on the Influence of GM, Roll Damping, and Above-Water Form on the Roll Response of Model 5613. Hydromechanics Department, Naval Surface Warfare Center Carderock Division, West Bethesda, Maryland, USA. Report NSWCCD-50-TR-2005/027.

Boccotti, P., 2000. Wave Mechanics for Ocean Engineering. Elsevier Science, Oxford. ISBN 9780080543727 496 pp.

Boccotti, P., 2014. Wave Mechanics and Wave Loads on Marine Structures. Butterworth-Heinemann, Elsevier, p. 344. https://doi.org/10.1016/C2013-0-13663-X.

Boos, D.D., Stefanski, L.D., 2013. Essential Statistical Inference: Theory and Method. Springer, p. 568. ISBN 978-1461448174.

Bretschneider, C.L., 1959. Wave Variability and Wave Spectra for Wind-Generated Gravity Waves. U.S. Army Beach Erosion Board, Washington, DC, USA. Technical Memorandum 118.

Bulian, G., Francescutto, A., 2004. A simplified modular approach for the prediction of the roll motion due to the combined action of wind and waves. J. Engineering for the Maritime Environment 218 (M3), 189–212.

Bulian, G., Francescutto, A., 2011. Effect of roll modelling in beam waves under multi-frequency excitation. Ocean Eng. 38, 1448–1463.

Bulian, G., Francescutto, A., 2011a. Considerations on Parametric Roll and Dead Ship Conditions for the Development of Second Generation Intact Stability Criteria. 12th Intl. Ship Stability Workshop, Washington, DC, USA, pp. 7–18.

Caldwell, J.B., Jang, Y.S., 1986. Risk and reliability analysis applied to ship capsize: a preliminary study. In: The Safeship Project, Ship Stability and Safety. Intl. Conf.

Campbell, B., Belenky, V., Pipiras, V., Sapsis, T., Weems, K., 2023. Estimation of probability of large roll angle with envelope peaks over threshold method. Ocean Eng. 290 (116296), this issue.

Choi, J., Jensen, J.J., 2019. Extreme value predictions using FORM for ship roll motions. Mar. Struct. 66, 52–65.

Coles, S., 2001. An Introduction to Statistical Modeling of Extreme Values. Springer, London. ISBN 1-85233-459-2.

Dudziak, J., Buczkowski, A., 1978. Probability of ship capsizing under the action of the beam wind and sea as a background of stability criteria. In: Polish Register of Ships, Prace Studialno-Roswojowe, Zeszyt Nr, vol. 13 (Gdansk, Poland).

Edwards, S.J., Troesch, A.W., Collette, M., 2021. Estimating extreme characteristics of stochastic non-linear systems. Ocean Eng. 233 (109042).

Embrechts, P., Klüppelberg, C., Mikosch, T., 2013. Modelling Extremal Events: for Insurance and Finance. Springer Science & Business Media. ISBN 978-3-642-33483-2.

Francescutto, A., 1998. On the statistical distribution of stochastic nonlinear rolling". In: Guedes-Soares, C. (Ed.), Risk and Reliability in Marine Technology. A. A. Balkema publishers, Rotterdam, Netherlands, pp. 107–116.

Francescutto, A., Naito, S., 2004. Large amplitude rolling in a realistic sea. Int. Shipbuild. Prog. 51 (No 2–3), 221–235.

Francescutto, A., Contento, G., Penna, R., 1994. Experimental evidence of strong nonlinear effects in the rolling motions of a destroyer in beam sea. In: Proc. 5th Intl. Conf. On Stability of Ships and Ocean Vehicles, (STAB 1994), vol. 1. Melbourne, Florida, USA.

Glotzer, D., Pipiras, V., Belenky, V., Campbell, B., Smith, T., 2017. Confidence interval for exceedance probabilities with application to extreme ship motions. REVSTAT Statistical J 15 (4), 537–563.

Glotzer, D., Pipiras, V., Belenky, V., Weems, K., Sapsis, T.P., 2024. Distributions and Extreme Value Analysis of Critical Response Rate and Split-Time Metric in Nonlinear Random Oscillators. Ocean Eng. (this issue).

Grimshaw, S.D., 1991. Calculating maximum likelihood estimates for the generalized Pareto distribution. In: Proc. 23rd Symp. Interface of Computing Science and Statistics, pp. 616–619. Seattle, Washington, USA.

Guth, S., Sapsis, T.P., 2022. Wave episode based Gaussian process regression for extreme event statistics in ship dynamics: between the Scylla of karhunen-loève convergence and the charybdis of transient features. Ocean Eng. 266 (112633) this issue.

Haddara, M.R., 1974. A modified approach for the application of fokker-plank equation to nonlinear ship motion in random waves. Int. Shipbuild. Prog. 21 (242), 283–288.

Haddara, M.R., Zhang, Y., 1994. On the joint probability density function of nonlinear rolling motion. J. Sound Vib. 169 (4), 562–569.

IMO IS Code, 2008. International Code on Intact Stability. London, UK, v+160 pp.

IMO MSC, 2020. 1/Circ.1627 Interim Guidelines on the Second Generation Intact Stability Criteria. London, December.

IMO MSC, 2023. 1/Circ.1652 Explanatory Notes to the Interim Guidelines on the Second Generation Intact Stability Criteria. London, April.

IMO SDC 8/INF, 2021. 2 Physical Background and Mathematical Models for Stability Failures of the Second Generation Intact Stability Criteria. Submitted by ITTC, London.

Iskandar, B.H., Umeda, N., 2001. Capsizing Probability of an Indonesian RoRo Passenger Vessel in Irregular Beam Seas (Third Report), vol. 190. J. of Society of Naval Architects of Japan.

Iskandar, B.H., Umeda, N., 2001a. Some examinations of capsizing probability calculations of Indonesian RoRo passenger ship in waves. J. of the Kansai Society of Naval Architects 236, 81–86.

Iskandar, B.H., Umeda, N., Hamamoto, M., 2000. Capsizing probability of an Indonesian RoRo passenger vessel in irregular beam seas. In: J. Of Society of Naval Architects of Japan, vol. 188, pp. 183–189.

Iskandar, B.H., Umeda, N., Hamamoto, M., 2001. Capsizing Probability of an Indonesian RoRo Passenger Vessel in Irregular Beam Seas (Second Report), vol. 189. J. of Society of Naval Architects of Japan.

Jensen, J.J., 2017. Efficient estimation of extreme non-linear roll motions using the first-order reliability method (FORM). J. Mar. Sci. Technol. 12 (4), 191–202.

Jensen, J.J., Capul, J., 2006. Extreme response predictions for jack-up units in second order stochastic waves by FORM. Probabilist. Eng. Mech. 21, 330–337.
Jensen, J.J., Choi, J., Nielsen, U.D., 2017. Statistical prediction of parametric roll using FORM. Ocean Eng. 144, 235–242.
Kim, M., Pipiras, V., Reed, A.M., Weems, K., 2023. Calibration of low-fidelity ship motion codes through regressions of high-fidelity forces. Ocean Eng. 290(116321) this issue.
Kim, D.H., Troesch, A.W., 2013. Statistical Estimation of Extreme Roll Responses in Short Crested Irregular Head Seas, vol. 121. Tr. SNAME.
Kim, D.H., Troesch, A.W., 2019. Stochastic wave inputs for extreme roll in near head seas. In: Belenky, V., Spyrou, K., van Walree, F., Neves, M.A.S., Umeda, N. (Eds.), Chapter 23 of *Contemporary Ideas On Ship Stability. Risk Of Capsizing*. Springer, pp. 393–405. ISBN 978-3-030-00514-6.
Kobylinski, L., 1975. Rational stability criteria and probability of capsizing. Paper 1.4. In: Proc. 1st Intl. Conf. On Stability of Ships and Ocean Vehicles (STAB 1975), p. 13. Glasgow, Scotland, UK.
Kougioumtzoglou, I., Spanos, P.D., 2014. Stochastic response analysis of the softening duffing oscillator and ship capsizing probability determination via a numerical path integral approach. Probabilist. Eng. Mech. 35, 67–74.
Kramer, H., Leadbetter, M.R., 1967. Stationary and Related Stochastic Processes. John Wiley, New York, p. 368.
Leadbetter, M.R., Lindgren, G., Rootzen, H., 1983. Extremes and related properties of random sequences and processes. In: Springer Series in Statistics. Springer-Verlag, New York-Berlin. ISBN 978-0-387-90731-4.
Lindgren, G., 2013. Stationary stochastic processes. In: Chapman & Hall/CRC Texts in Statistical Science Series. CRC Press, Boca Raton, Florida, USA, Theory and applications. ISBN 9781466557796.
Mager, J., 2015. *Automatic Threshold Selection of the Peaks over Threshold Method*. Master's Thesis. Technische Universitat Munchen, Germany.
Maki, A., 2017. Estimation method of the capsizing probability in irregular beam seas using non-Gaussian probability density function. J. Mar. Sci. Technol. 22 (2), 351–360.
Maki, A., Umeda, N., Matsuda, A., Yoshizumi, H., 2019. Non-Gaussian PDF of ship roll motion in irregular beam sea and wind conditions-comparison between theory and experiment. Ocean Eng. 188, 106278.
Maki, A., Dostal, L., Maruyama, Y., Sasa, K., Sakai, M., Umeda, N., 2022. Enhanced estimation method and approximation method of the PDF of roll angular acceleration and jerk in beam seas. this issue Ocean Eng. 264, 7, 112159.
McTaggart, K.A., 2000. Ongoing work examining capsize risk of intact frigates using time domain simulation. In: Vassalos, D., Hamamoto, M., Papanikolaou, A., Molyneux, D. (Eds.), Contemporary Ideas of Ship Stability. Elsevier, pp. 587–595. ISBN 978-0080436524.
McTaggart, K.A., de Kat, J.O., 2000. Capsize risk of intact frigates in irregular seas. Trans. SNAME 108, 147–177.
Mohamad, M.A., Sapsis, T., 2018. Sequential sampling strategy for extreme event statistics in nonlinear dynamical systems. Proc. of the Natl. Acad. of Sciences of United States of America PNAS 115, 11138–11143.
Mohamad, M.A., Cousins, W., Sapsis, T., 2016. A probabilistic decomposition-synthesis method for the quantification of rare events due to internal instabilities. J. Comput. Phys. 322, 288–308.
Naess, A., Moe, V., 2000. Efficient path integration methods for nonlinear dynamic systems. Probabilist. Eng. Mech. 15, 221–231.
Nechaev, Y.I., 1989. Modelling of Ship Stability in Waves. Sudostroenie, Leningrad, p. 240 (in Russian).
Nekrasov, V.A., 1994. Stochastic stability theory of ship motion. Proc. of 5th Intl. Conf. on Stability of Ships and Ocean Vehicles (STAB 1994 5 (Melbourne, Florida, USA).
Paroka, D., Umeda, N., 2006. Capsizing probability prediction of the large passenger ship in irregular beam wind and waves: comparison of analytical and numerical methods. J. Ship Res. 50 (4), 371–377.
Paroka, D., Okura, Y., Umeda, N., 2006. Analytical prediction of capsizing probability of a ship in beam wind and waves. J. Ship Res. 50 (2), 187–195.
Pearson, K., 1916. Contributions to the mathematical theory of evolution, X: second supplement to a memoir on skew variation. Phil. Trans. of the Royal Society 216, 429–457. https://doi.org/10.1098/rsta.1916.0009.
Peters, W., Belenky, V., 2023. On regulatory consistency of criteria for dead ship condition and pure loss of stability. In: Spyrou, K., Belenky, V., Katayama, T., Bačkalov, I., Francescutto, A. (Eds.), Chapter 4 of *Contemporary Ideas On Ship Stability – from Dynamics To Criteria*. Springer, pp. 73–92. ISBN 978-3-031-16328-9.
Pickands, J., 1975. Statistical inference using extreme order statistics. Ann. Stat. 3 (1), 119–131.
Pipiras, V., 2020. Pitfalls of data-driven peaks-over-threshold analysis: perspectives from extreme ship motions. Probabilist. Eng. Mech. 60, 103053.
Rainey, R.C.T., Thompson, J.M.T., Tam, G.W., Noble, P.G., 1990. The transient capsize diagram — a route to soundly-based new stability regulations. In: Proc. Of 4th Intl. Conf. on Stability of Ships and Ocean Vehicles (STAB 1990), vol. 2, pp. 613–619. Naples, Italy.
Rasmussen, C.E., Williams, C.K.I., 2006. Gaussian Processes for Machine Learning. the MIT Press, Cambridge, Massachusetts, USA, p. 248. ISBN 0-262-18253-X.
Reed, A.M., 2021. Predicting extreme loads and the processes for predicting them efficiently. In: Proc. 1st Intl. Conf. On Stability and Safety of Ships and Ocean Vehicles (STABS) (Glasgow, Scotland, UK).
Reiss, R.D., Thomas, M., 2007. Statistical Analysis of Extreme Values with Application to Insurance, Finance, Hydrology and Other Fields, third ed. Birkhäuser Verlag, Basel, p. 529. ISBN 978-3764372309.
Sevastianov, N.B., 1963. On Probabilistic Approach to Stability Standards, vol. 18. Trans. of Kaliningrad Institute of Technology, Kaliningrad, pp. 3–12 (in Russian).
Sevastianov, N.B., 1982. Probabilistic stability regulation as a problem of reliability theory. Leningrad Transactions of Russian Register Shipping 12, 94–100 (in Russian).
Sevastianov, N.B., 1994. An algorithm of probabilistic stability assessment and standards. Proc. of 5th Intl. Conf. on Stability of Ships and Ocean Vehicles (STAB 1994 5 (Melbourne, Florida, USA).
Shigunov, V., 2023. Extrapolation of failure rate over wave height. Ocean Eng. 272 (113801) this issue.
Shin, Y.S., Belenky, V.L., Lin, W.M., Weems, K.M., Engle, A.H., 2003. Nonlinear time domain simulation technology for seakeeping and wave-load analysis for modern ship design. SNAME Trans 111, 557–578.
Silva, K.M., Maki, K.J., 2021. Towards a computational fluid dynamics implementation of the critical wave groups method". Ocean Eng. 235, 10, 109451.
Silva, K.M., Maki, K.J., 2024. Implementation of Critical Wave Groups Method with Computational Fluid Dynamics and Neural Networks. Ocean Eng., 292(116468), this issue.
Smith, R.L., 1987. Estimating tails of probability distributions. Ann. Stat. 15, 1174–1207.
Sólnes, J., 1997. Stochastic Processes and Random Vibrations: Theory and Practice. Wiley, New York, New York, USA. ISBN: 978-0-471-97192-4.
Spyrou, K.J., 2009. Pure-loss of Stability Revisited: Analytical Design Aid. Internal Report of National Technical University of Athens, Greece.
Spyrou, K.J., Tigkas, I.G., 2007. Principle and application of continuation methods for ship design and operability analysis. In: *Proc. 10th Intl. Symp. On Practical Design Of Ships And Other Floating Structures* (PRADS 2007), pp. 388–395. Houston, Texas, USA.
Spyrou, K.J., Belenky, V., Reed, A., Weems, K., Themelis, N., Kontolefas, I., 2014. Split-Time Method for Pure Loss of Stability and Broaching-To *Proc. 30th Symp. Naval Hydrodynamics*. Hobart, Tasmania, Australia.
Stephens, M.A., 1974. EDF statistics for goodness of *t* and some comparisons. J. Am. Stat. Assoc. 69 (347), 730–737.
Su, Z., Falzarano, J., 2013. Markov and melnikov based methods for vessel capsizing criteria. Ocean Eng. 64, 146–152.
Thanou, A.A., 2010. Probabilistic consideration of the weather criterion of ship stability. In: Final Year Diploma Thesis (Supervised by K. J. Spyrou). National Technical University of Athens, Greece.
Themelis, N., Spyrou, K.J., 2007. Probabilistic assessment of ship stability. Tr. SNAME 115, 181–206.
Themelis, N., Spyrou, K.J., 2008. Probabilistic assessment of ship stability based on the concept of critical wave groups. In: Proc. Of the 10th Intl. Ship Stability Workshop, pp. 115–125. Daejeon, Korea.
Tonguć, E., Söding, H., 1986. Computing capsizing frequencies of ships in a seaway. In: Proc. 3rd Intl. Conf. On Stability of Ships and Ocean Vehicles (STAB 1986), vol. 2. Addendum 1, Gdansk, Poland, pp. 51–60.
Umeda, N., Yamakoshi, Y., 1994. Probability of ship capsizing due to pure loss of stability in irregular quartering seas. Naval Architecture and Ocean Engineering 30, 73–85.
Umeda, N., Yamakoshi, Y., Tsuchiya, T., 1990. Probabilistic study on ship capsizing due to pure loss of stability in irregular quartering seas. In: *Proc. Of 4th Intl. Conf. on Stability Of Ships And Ocean Vehicles (STAB 1990)*, Naples, Italy, vol. 1, pp. 328–335.
Wandji, C., 2023. Review of probabilistic methods for direct dynamic stability of ships in random seaway. In: Spyrou, K., Belenky, V., Katayama, T., Bačkalov, I., Francescutto, A. (Eds.), Contemporary Ideas on Ship Stability – from Dynamics to Criteria. Springer Series Fluid Mechanics and Its Application, pp. 189–209. ISBN 978-3-031-16328-9.
Wandji, C., Shigunov, V., Pipiras, V., Belenky, V., 2024. Benchmarking of Direct Counting Approaches. Ocean Eng, this issue.
Weems, K., Belenky, V., 2017. Including diffraction and radiation into probabilistic description of capsizing. In: In: Proc. 16th Intl. Ship Stability Workshop, Belgrade, Serbia, pp. 117–123.
Weems, K., Belenky, V., 2023. Volume-base reduced-order model for ship motions. this issue Ocean Eng. 289 (116214). this issue.
Weems, K., Wundrow, D., 2013. Hybrid models for fast time-domain simulation of stability failures in irregular waves with volume-based calculations for froude-krylov and hydrostatic force. In: Proc. Of 13th Intl. Ship Stability Workshop. Brest, France, pp. 130–137.
Weems, K., Lin, W.M., Zhang, S., Treakle, T., 2000. Time domain prediction for motions and loads of ships and marine structures in large seas using a mixed-singularity formulation. In: Proc. Osaka Colloquium on Seakeeping and Stability of Ships (OC2000) (Osaka, Japan).
Weems, K., Belenky, V., Spyrou, K., 2018. Numerical simulations for validating models of extreme ship motions in irregular waves. In: Proc. 32nd Symp. Naval Hydrodynamics, Hamburg, Germany.
Weems, K., Sapsis, T., Pipiras, V., 2022. Development of Reduced Order Models for Hydrodynamic Responses. Proc. 18th Intl. Ship Stability Workshop, Gdansk, Poland, pp. 285–294.
Weems, K., Belenky, V., Campbell, B., Pipiras, V., 2023. Statistical validation of the split-time method with volume-based numerical simulation. In: Spyrou, K., Belenky, V., Katayama, T., Bačkalov, I., Francescutto, A. (Eds.), Chapter 13 of *Contemporary Ideas On Ship Stability – from Dynamics To Criteria*. Springer, pp. 225–243. ISBN 978-3-031-16328-9.